THE SOFT SPHERE MODEL FOR NUCLEAR QUADRUPOLE RESONANCE IN RARE EARTH TRICHLORIDES UNDER HYDROSTATIC PRESSURE

Thesis for the Degree of Ph. D.
MICHIGAN STATE UNIVERSITY
DAVID HARLAN CURRENT
1971

This is to certify that the

thesis entitled

The Soft Sphere Model for Nuclear Quadrupole Resonance in Rare Earth Trichlorides Under Hydrostatic Pressure

presented by

David Harlan Current

has been accepted towards fulfillment of the requirements for

Ph.D. degree in Physics

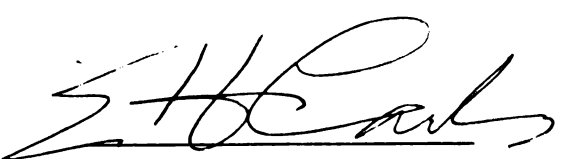

Major professor

Edward H. Carlson

Date August 23, 1971

O-7639

ABSTRACT

THE SOFT SPHERE MODEL FOR NUCLEAR QUADRUPOLE RESONANCE IN RARE EARTH TRICHLORIDES UNDER HYDROSTATIC PRESSURE

by

David Harlan Current

We have measured the nuclear quadrupole resonance of ^{35}Cl in $CeCl_3$, $PrCl_3$, $NdCl_3$, $SmCl_3$ and $GdCl_3$ at 77K as a function of hydrostatic pressure. Pressure was generated with a helium gas piston system and measured with a Bourdon gauge. Quadrupole resonance frequencies were measured with a simple pulsed spectrometer having a resolution of better than one kHz. In each compound the quadrupole resonance frequency in a linear function of pressure up to at least a pressure of 4.5×10^3 kg/cm^2. In all cases the coefficient $\nu_o^{-1} (\partial\nu/\partial P)_T$ is negative; the frequencies decrease with pressure. The coefficient decreases in magnitude from $-5.59\pm0.02 \times 10^{-6}$ cm^2/kg for $CeCl_3$ to $-3.86\pm0.02 \times 10^{-6}$ cm^2/kg for $GdCl_3$. This contradicts the point charge model of electric field gradients applied to these compounds. We introduce the soft sphere model of electric field gradients. This model includes the effects of molecular overlap on the electric field gradient by subtracting from the point charge contribution of near neighbor ions a term of the form $q_o = F \exp[(R_{ij}-R)/\rho_{ij}]$. This form for the overlap contribution is deduced from Hartree-Fock, Self-Consistent-Field (HF-SCF) calculations by Matcha[1] on the KCl molecule. The soft sphere parameters are assumed to obey Gilbert's[2] additivity rules $R_{ij} = R_i + R_j$ and $\rho_{ij} = \rho_i + \rho_j$;

a Hartree-Fock-Slater calculation of ionic wavefunctions is utilized to obtain their values.[3] The Sternheimer antishielding factor, $(1 - \gamma_\infty)$, and the overlap strength, F, are taken as adjustable parameters to fit the zero pressure frequency and asymmetry parameters of $GdCl_3$. For the choices $R_{Cl} = 2.740$ bohr and $\rho_{Cl} = 0.429$ bohr the values of the overlap strength and antishielding parameter necessary to fit the observed quadrupole frequency and asymmetry parameter in $GdCl_3$ are $F = 0.5695$ bohr^{-3} and $1 - \gamma_\infty = 30.95$. The model then predicts the quadrupole frequency in $LaCl_3$ to within 2.5% of the measured value and the frequency and asymmetry parameter in $PrCl_3$ to within 0.2% and 0.5% of the measured values. Because the compressibility of these compounds is unknown it is difficult to compare the predictions of the soft sphere model with the observed pressure dependence of the quadrupole frequencies. For volume decreasing faster along the a-axis than along the c-axis the model is in qualitative agreement with experiment.

[1]Robert L. Matcha, J. Chem. Phys. 53, 485 (1970).

[2]T. L. Gilbert, J. Chem. Phys. 49, 2640 (1968).

[3]F. Herman and S. Skillman, Atomic Structure Calculations, Prentice Hall, Englewood Cliffs, New Jersey, 1963.

THE SOFT SPHERE MODEL FOR NUCLEAR QUADRUPOLE RESONANCE IN RARE EARTH TRICHLORIDES UNDER HYDROSTATIC PRESSURE

by

David Harlan Current

A THESIS

Submitted to
Michigan State University
in partial fulfillment of the requirements
for the degree of

DOCTOR OF PHILOSOPHY

Department of Physics

1971

DEDICATION

To my wife Diane, who has been exceedingly patient and understanding and who has learned to wake up late at night, and to my son Michael, who has finally learned not to wake up late at night, I dedicate this thesis.

ACKNOWLEDGMENTS

I wish to express my appreciation to Professor E. H. Carlson who not only suggested this thesis topic to me and assisted in the development of some of the ideas therein, but who also provided constant stimulation and guidance. I wish also to thank Professor C. L. Foiles, in whose laboratory most of the experimental work was performed, for valuable assistance with the high pressure apparatus and many illuminating discussions.

Dr. J. P. Hessler assisted with some of the data collection and provided many valuable comments. Nancy Hessler spent long hours typing the manuscript. Charles Butterfield performed the HFS calculations from which the soft sphere parameters were deduced.

Finally I wish to thank Central Michigan University for a two year leave of absence during which this work was completed.

TABLE OF CONTENTS

Page

LIST OF TABLES

LIST OF FIGURES

I. INTRODUCTION

An atomic nucleus with spin greater than 1/2 can have a nonspherical distribution of nuclear charge and hence a nuclear quadrupole moment Q. This quadrupole moment will couple to an electric field gradient to produce a splitting of the energy levels labeled by the z-component of the nuclear spin. The electric field gradient is a traceless second rank tensor characterized by a magnitude q, an asymmetry parameter, η, which is a measure of the tensors departure from cylindrical symmetry, and the three Euler angles which specify the orientation of its principal axes. The nuclear quadrupole coupling constant, eQq/h, where e is the electronic charge, h is Planck's constant and q is the magnitude of the electric field gradient, can be measured experimentally by inducing transitions from one energy level to another. This technique is known as nuclear quadrupole resonance. The theory of quadrupole resonance is reviewed in Chapter II. If the nuclear quadrupole moment is known from other measurements, then from the quadrupole coupling constant one can determine the field gradient at the nuclear position.

The electric field gradient components can be expressed in spherical tensor notation as

$$q_m = \int r^{-3} \rho(\vec{r}) Y_2^m (\theta,\phi) d\vec{r} \ ,$$

where $Y_2^m (\theta,\phi)$ is a spherical harmonic, and $\rho(\vec{r})$ is the electronic charge density. This form emphasizes that the electric field gradient gives a description of the electronic charge distribu-

tion in the neighborhood of the nucleus. Since only that part of $\rho(\vec{r})$ with the symmetry of Y_2^m makes a contribution to the field gradient, there is no contribution from the spherically symmetric part of $\rho(\vec{r})$. Most of the contribution to the electric field gradient at the nucleus of a given ion comes from the outer, nonspherical part of the ion as well as from other nearby ions. Thus nuclear quadrupole resonance provides an excellent experimental tool for investigating the electronic charge density at nuclear sites in solids.

The compounds studied in this work, the trichlorides of lanthanum through gadolinium, all have the same hexagonal structure. An excellent x-ray study of these compounds has recently been reported (Morosin, 1968). The geometry (ion-ion distances and angles) varies slowly from one compound to another. In addition whatever properties of the rare earth ions that are important in determining the electric field gradient are also expected to be a slowly varying function of cation species. The ^{35}Cl resonances in these compounds have all been reported previously: in $PrCl_3$ by Hughes, Montgomery, Moulton and Carlson (1964); in $GdCl_3$ by Carlson (1966); in $CeCl_3$, $NdCl_3$ and $SmCl_3$ by Mangum and Utton (1967); and in $LaCl_3$ by Carlson and Adams (1969). No quadrupole resonances in $PmCl_3$ or $EuCl_3$ have been measured. Although a large amount of experimental data on quadrupole resonances in ionic salts is available, very few of these compounds have well determined structures. The hexagonal rare earth trichlorides are an important exception and provide an excellent opportunity to test theories of the electric field gradient in ionic salts.

The earliest attempt to calculate the electric field gradient in an ionic solid was the point charge model of Bersohn (1958). This model assumes that the effect of each ion in the crystal can be represented by a point charge located at the position of each ion. The electric field gradient at any ion is obtained by summing the contributions of all other ions in the crystal. Bersohn calculated the electric field gradient at Na^{+} in $NaNO_3$, $NaClO_3$ and $NaBrO_3$ as well as the electric field gradient at Cu^{2+} in CuO_2 and at Al^{3+} in Al_2O_3. Carlson and Adams (1969) have applied the point charge model to the rare earth trichlorides. Throughout its history the point charge model has enjoyed rather limited success. It seems to do a better job of predicting the field gradient at positive ions than at negative ions. Burns (1959) and others (Brun and Hofer, 1962; Raymond, 1971) have attempted to expand the point charge model by including higher multipole contributions from polarized ions. Their attempts have not always been very successful.

In an effort to obtain additional information on the electric field gradient in the rare earth trichlorides we have measured the quadrupole resonance frequency as a function of hydrostatic pressure. The application of hydrostatic pressure changes the geometry of the unit cell, and these geometrical changes are reflected in a change in the electric field gradient. The details of the experiments are discussed in Chapter III.

It is well known that molecular overlap produces a significant contribution to the electric field gradient (Das and Karplus, 1964). In Chapter IV we introduce the soft sphere model of electric field gradients. This model includes a systematic parameterization of the overlap contribution to electric field gradients. We then use the model to calculate the zero pressure quadrupole coupling constants for the rare earth trichlorides. We find substantial agreement with the experimental results. In applying the model to the pressure dependence of the quadrupole frequencies in these compounds, we are hampered by the lack of experimental data on the compressibilities. However the model is in qualitative agreement with the high pressure experiments.

II. QUADRUPOLE RESONANCE IN THE HEXAGONAL RARE EARTH TRICHLORIDES

A. Quadrupole Hamiltonian

The Hamiltonian for the interaction of the electric quadrupole moment of a nucleus with an electric field gradient due to charges external to the nucleus can be written as (Das and Hahn, 1958)

$$H_Q = \overleftrightarrow{Q} : \overleftrightarrow{\nabla E} = \sum_m Q_2^m \, (\nabla E)_2^{-m} \, . \tag{2.1}$$

Q_2^m are the irreducible components of the nuclear quadrupole charge distribution operator and $(\nabla E)_2^m$ are the irreducible components of the electric field gradient operator evaluated at the nuclear position. In terms of the nuclear quadrupole moment, Q, the components of $\overleftrightarrow{Q}$ are given by Das and Hahn (1958) as

$$Q_2^0 = \frac{2eQ}{4I(2I-1)} \, [3I_z^2 - I^2], \tag{2.2}$$

$$Q_2^{\pm 1} = \frac{\sqrt{6}eQ}{4I(2I-1)} \, [I_z I_\pm + I_\pm I_z], \tag{2.3}$$

and

$$Q_2^{\pm 2} = \frac{\sqrt{6}eQ}{4I(2I-1)} \, (I_\pm)^2. \tag{2.4}$$

The coordinates of the nuclear spin operators are taken in some arbitrary Cartesian frame.

In the same frame the field gradient has components

$$V_{ij} = \frac{\partial^2 V}{\partial x_i \partial x_j} \qquad (i,j = x,y,z), \tag{2.5}$$

where V is the electrostatic potential at the nucleus. V_{ij} is symmetric and, if V is produced by charges exterior

to the nucleus, traceless. If the Cartesian frame is chosen so as to diagonalize V_{ij}, then the components of the field gradient operator are given by

$$(\nabla E)^0_2 = \frac{1}{2} V_{zz} , \qquad (\nabla E)^{\pm 1}_2 = 0 \tag{2.6}$$

and

$$(\nabla E)^{\pm 2}_2 = \frac{1}{2\sqrt{6}} (V_{xx} - V_{yy}) . \tag{2.7}$$

If we assume that $|V_{xx}| \leq |V_{yy}| \leq |V_{zz}|$, and define the field gradient, q, and asymmetry parameter, η, by

$$eq = V_{zz} \quad \text{and} \quad \eta = (V_{xx}-V_{yy})/V_{zz}, \tag{2.8}$$

then

$$(\nabla E)^0_2 = \frac{1}{2} eq \quad \text{and} \quad (\nabla E)^{\pm 2}_2 = \frac{1}{2\sqrt{6}} \eta eq. \tag{2.9}$$

By carrying out the sum in the Hamiltonian one arrives at

$$H_Q = A[3I_z^2 - I^2 + \frac{1}{2} \eta (I_+ I_+ + I_- I_-)], \tag{2.10}$$

where

$$A = \frac{e^2 qQ}{4I(2I-1)} . \tag{2.11}$$

A complete derivation of this result is given by Slichter (1963).

The matrix elements of this Hamiltonian taken between nuclear angular momentum states are

$$\begin{aligned} \langle I_{m'} | H_Q | I_m \rangle &= A[3m^2 - I(I+1)] \, \delta_{m',m} \\ &+ \tfrac{1}{2}\eta A \sqrt{[I(I+1)-m(m+1)][I(I+1)-(m+1)(m+2)]} \, \delta_{m',m+2} \\ &+ \tfrac{1}{2}\eta A \sqrt{[I(I+1)-m(m-1)][I(I+1)-(m-1)(m-2)]} \, \delta_{m',m-2} . \end{aligned} \tag{2.12}$$

For I = 3/2 the non-zero elements are

$$\langle \tfrac{3}{2}, \pm\tfrac{3}{2} | H_Q | \tfrac{3}{2}, \pm\tfrac{3}{2} \rangle = 3A \ , \tag{2.13}$$

$$\langle \tfrac{3}{2}, \pm\tfrac{1}{2} | H_Q | \tfrac{3}{2}, \pm\tfrac{1}{2} \rangle = -3A \tag{2.14}$$

and

$$\langle \tfrac{3}{2}, \pm\tfrac{3}{2} | H_Q | \tfrac{3}{2}, \pm\tfrac{1}{2} \rangle = \sqrt{3}\eta A \ , \tag{2.15}$$

with

$$A = e^2qQ/12 \ . \tag{2.16}$$

The Hamiltonian is easily diagonalized and yields two doubly degenerate energy levels with eigenvalues

$$E_\pm = 3A\sqrt{1 + \tfrac{1}{3}\eta^2} \ . \tag{2.17}$$

Thus there is a single quadrupole resonance transition with frequency given by

$$h\nu_Q = E_+ - E_- \tag{2.18}$$

$$\nu_Q = \frac{e^2qQ}{2h}\sqrt{1 + \tfrac{1}{3}\eta^2} \ . \tag{2.19}$$

B. Crystal Structure

The trichlorides of lanthanum through gadolinium were shown to be isostructural by Bommer and Hohmann (1941). Zachariasen (1948) showed that they were isomorphic to UCl_3 with space group $P6_3/m$, and measured the lattice constants A and C. In this structure there are two molecules per unit cell with metal ions at ±(1/3, 2/3, 1/4) and chloride ions at ±(u, v, 1/4), ±(-v, u-v, 1/4) and ±(v-u, -u, 1/4). Zachariasen measured the chloride positional parameters, u and v, only for UCl_3.

Templeton and Dauben (1954) measured the lattice constants for the entire series (with the exception of $LaCl_3$). Morosin (1968) measured lattice constants and chloride positional parameters for $LaCl_3$, $NdCl_3$, $EuCl_3$ and $GdCl_3$. Lattice constants and positional parameters for $CeCl_3$, $PrCl_3$ and $SmCl_3$ have been estimated from Morosin's data. The procedure is described in Appendix A.

The volume of the unit cell varies smoothly across the series with a minimum at $GdCl_3$. The volume per chloride ion (cell volume divided by six) ranges from 35.20 $\mathring{A}^3$ for $LaCl_3$ to 32.16 $\mathring{A}^3$ for $GdCl_3$. The crystal structure data is summarized in Table 2.1.

In these crystals all ions lie on mirror planes perpendicular to the c-axis. Figure 2.1 shows two layers of $GdCl_3$. The large spheres are Cl^- (radius 1.8 $\mathring{A}$) and the small spheres are Gd^{3+} (radius 1.2 $\mathring{A}$). The radii are taken from Pauling (1940). For the chloride labeled o the three nearest metal ions are labeled a and b, and the eight nearest chloride ions are labeled c, d and e. We have chosen a coordinate system centered at ion o with the z-axis parallel to the crystal c-axis and the y-axis bisecting the 120° angle of the unit cell. In Figure 2.1 the z-axis is out of the plane of the paper and the x-axis and y-axis are horizontal and vertical respectively. The positions of the eleven nearest ions are summarized in Table 2.2.

The existence of the mirror plane perpendicular to the c-axis requires that one of the principal axes of

Table 2.1. Structure Data

Compound	A(Å)	C(Å)	u	v	V/cell(Å^3)	V/Cl$^-$(Å^3)
$LaCl_3$[a]	7.4779	4.3745	0.38741	0.30155	211.84[c]	35.31
$CeCl_3$[b]	7.452	4.328	0.38753	0.30160	208.14	34.69
$PrCl_3$[b]	7.425	4.283	0.38765	0.30164	204.49	34.08
$NdCl_3$[a]	7.3988	4.2423	0.38777	0.30167	201.12	33.52
$SmCl_3$[b]	7.384	4.164	0.38852	0.30172	196.62	32.77
$EuCl_3$[a]	7.3746	4.1323	0.38911	0.30174	194.63	32.44
$GdCl_3$[a]	7.3663	4.1059	0.38929	0.30153	192.95	32.16

[a]Data from Morosin (1968).

[b]Estimated from Morosin's data. See Appendix A.

[c]Morosin's value is incorrect.

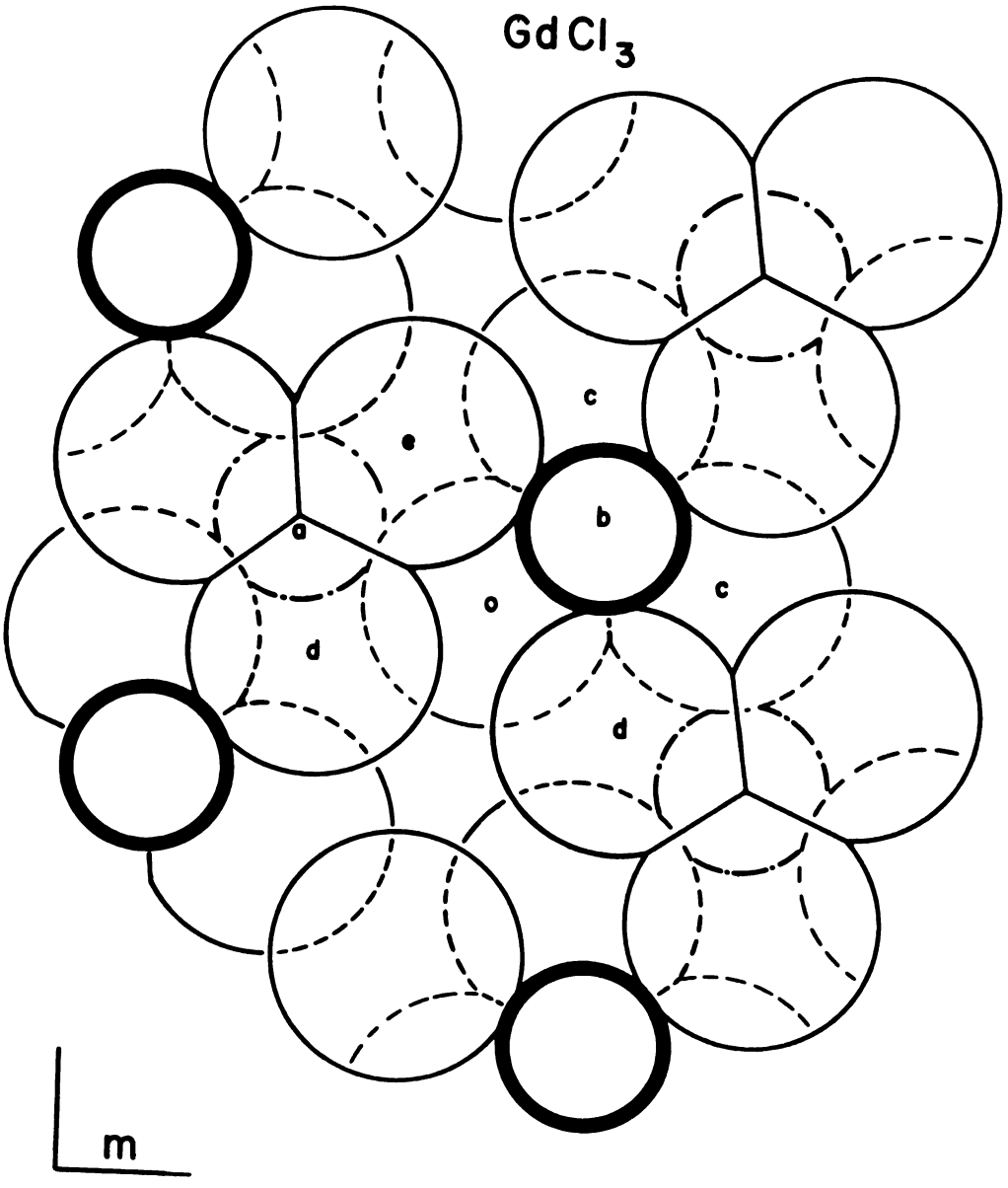

Figure 2.1. $GdCl_3$ Structure

Table 2.2. Locations of Near Ions in $GdCl_3$

Species	Label[a]	R(Å)	X(Å)	Y(Å)	Z(Å)
Gd^{3+}	a	2.9177	-2.6863	1.1388	0.0000
Gd^{3+}	b	2.8223	1.5666	1.1388	±2.0529
Cl^-	c	3.3546	3.3361	0.3514	0.0000
Cl^-	c	3.3546	1.3637	3.0649	0.0000
Cl^-	d	3.3169	-2.4834	-0.7873	±2.0529
Cl^-	d	3.3169	1.9236	-1.7570	±2.0529
Cl^-	e	3.2643	-1.1197	2.2775	±2.0529

[a]Labeled in Figure 2.1.

the electric field gradient at each chloride ion be along the c-axis. Experimentally this has been shown to be V_{xx} (Hughes, et al., 1964). All three chloride ions in the molecule are chemically equivalent. That is, the diagonal elements of the electric field gradient tensor are the same at each ion, and there is a single pure quadrupole frequency, but the orientation of the tensors differs by 120°. In addition, since the crystals lack a two fold axis in the mirror plane, it is not easily possible to determine one end of the c-axis from the other (Carlson and Adams, 1969). Thus the orientation of the electric field gradient principal axes can only be experimentally measured to within a multiple of 60°. For these reasons we have not attempted to calculate the orientation of the principal axes, except to be sure that V_{xx} was always along the c-axis.

C. Experimental Results at One Atmosphere Pressure

^{35}Cl nuclear quadrupole resonance frequencies have been reported for all of the hexagonal rare earth trichlorides with the exception of $PmCl_3$ and $EuCl_3$. Asymmetry parameters have been accurately measured only for $PrCl_3$ and $GdCl_3$. The experimental data is summarized in Table 2.3.

Table 2.3. Experimental NQR Frequencies and Asymmetry Parameters

Compound	η	ν(MHz)$_{4K}$	ν(MHz)$_{77K}$	ν(MHz)$_{300K}$
$LaCl_3$	---	4.167	---	---
$CeCl_3$	---	4.387	4.377	4.341
$PrCl_3$	.4937	4.567	4.562	---
$NdCl_3$	---	4.729	4.722	4.676
$SmCl_3$	---	5.033	5.027	4.976
$GdCl_3$	.4265	5.315	5.308	5.248

Uncertainties are 1 in the last figure. η's are measured at T<4K and are taken from Hessler (1971). Frequencies at 4K are taken from Carlson and Adams (1969).

III. EXPERIMENTAL TECHNIQUES AND RESULTS

A. Sample Preparation

Anhydrous rare earth trichloride powder purchased from Lindsay was used in the preparation of single crystal samples. Our laboratory method is similar to that described by Garton, et al. (1964). The powder was melted and distilled under vacuum into a Vycor growing tube, which was then slowly lowered through a gradient furnace. The only exception was $SmCl_3$; the powder was not distilled but merely melted in the presence of HCl gas and allowed to flow into the growing tube. As the crystals are hydroscopic, they are stored under mineral oil when removed from the growing tube.

Small samples were prepared for resonance measurements by cutting single crystals perpendicular to the c-axis on a diamond saw to a length of about 1/2 inch. The resulting pieces are then cleaved parallel to the c-axis to yield hexagonal samples about 1/8 inch in diameter. The samples were coated with a thin layer of GE7031 cement for protection against moisture.

B. The Spectrometer

The spectrometer used in this work was a simple pulsed instrument developed by Parks (1967), and referred to as "the minipulser". A pulse of radio frequency power derived from an external oscillator is applied to a coil wrapped directly on the sample. The pulse amplitude is about 200 volts, the pulse length about 25 microseconds, and the

repetition rate a few milliseconds. In this work the coil axis was parallel to the c-axis of the sample. The same coil acts as a receiver to pick up the induced signal from the sample. This signal is amplified, multiplied by the signal from the external oscillator, and displayed on an oscilloscope. The quadrupole resonance frequency is determined by adjusting the oscillator frequency until a zero beat condition is observed. The oscillator frequency is monitored continuously with an electronic counter.

The minipulser has several advantages for this work. Signals are strong enough so that direct oscilloscope display is possible without the need for signal averaging techniques. Frequency measurements can be made rapidly and with high precision (frequency differences of 100Hz can be resolved). In addition, if one is willing to sacrifice some loss of signal strength, a relatively large input capacitance (of the order of 500 p.f.) can be tolerated.

C. High Pressure Apparatus

A schematic diagram of the experimental apparatus is shown in Figure 3.1. Figure 3.2 shows details of the BeCu pressure cell. The high pressure gas seal between the two halves of the cell is made with a series of stainless steel rings which are coated with a thin layer of indium (Goree, et al., 1965). These rings provided an excellent seal and could be reused at least six times without

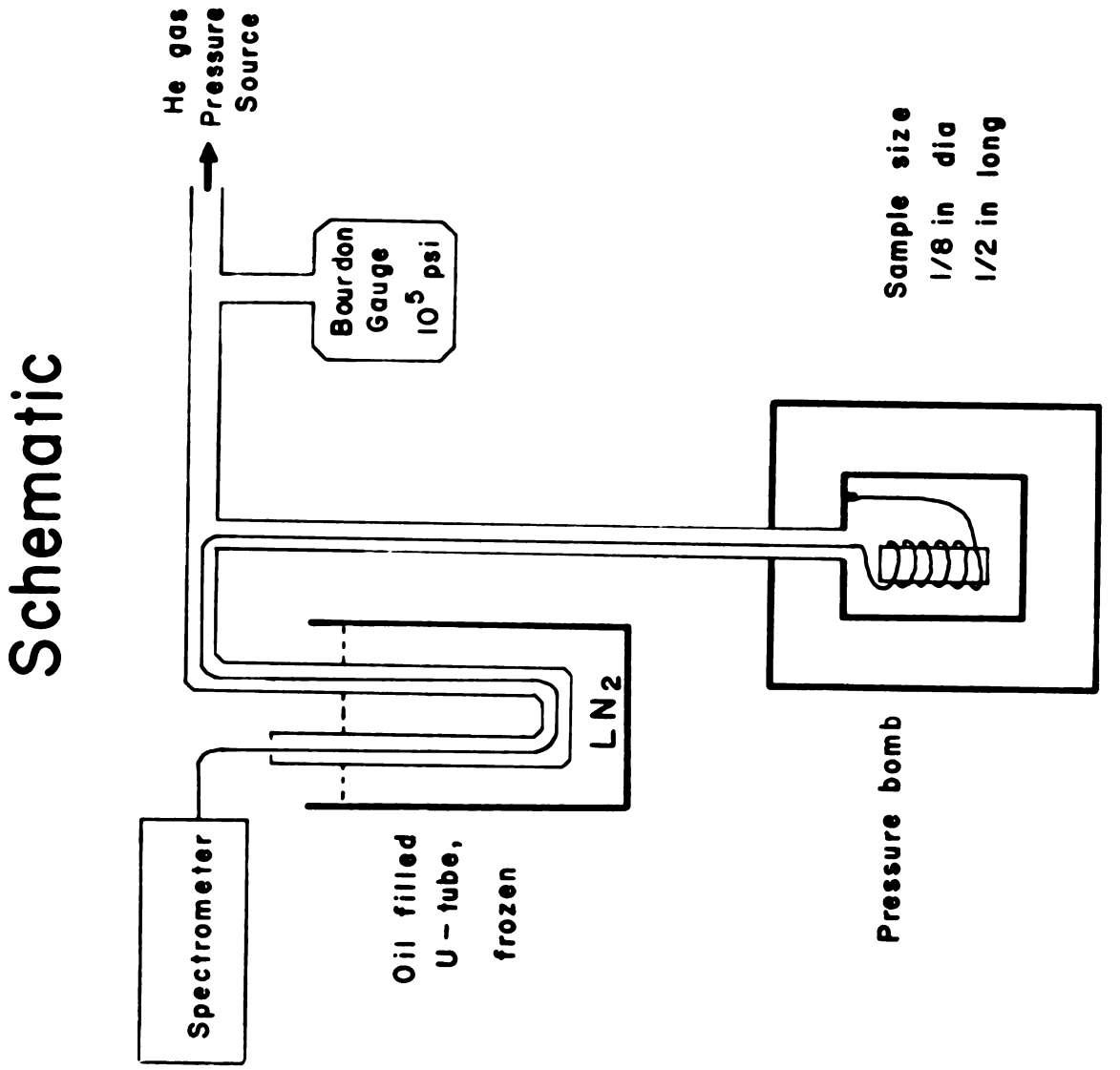

Figure 3.1. Schematic Diagram of Experimental Apparatus

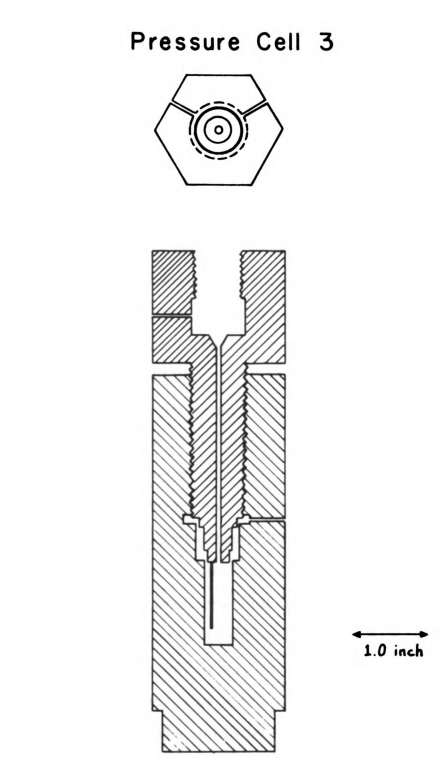

Figure 3.2. High Pressure Cell

recoating. The upper half of the cell is connected to 5/16 o.d. by 1/16 i.d. stainless steel, high pressure tubing by a standard cone seal.

The high pressure tubing is electrically grounded and serves as a shield for the spectrometer lead. The lead is extracted from the high pressure region through a U-shaped tube, approximately 20 inches deep, filled with Dow Corning 704 silicone diffusion pump oil. When frozen in liquid nitrogen, the oil expands and provides a seal which easily withstands pressures up to 90,000 pounds per square inch. However, some care must be taken to be sure that there are no trapped bubbles of air in the oil before it is frozen.

Hydrostatic pressure is generated in helium gas by an oil driven piston and a 10:1 intensifier. The gas is slowly admitted to the system through a liquid nitrogen cooled trap to remove impurities. Pressure was measured with a Bourdon gauge. The manufacturer claims 2% accuracy for this gauge. Although no absolute calibration was attempted, the gauge has been checked against manganin resistance data to verify the manufacturer's claim.

Our experimental procedure was to wrap the sample with a suitable coil (generally about 20 turns of #36 Cu wire) and mount it in the pressure cell. The cell and oil seal were then attached to the rest of the pressure apparatus and the oil seal slowly frozen. With the cell at room temperature the spectrometer was adjusted and the pressure was raised to approximately 80,000 p.s.i. When

a signal could be seen, room temperature data was taken. The pressure was then reduced to about 15,000 p.s.i. and the cell immersed in liquid nitrogen. We allowed at least 30 minutes for thermal equilibrium to be established before taking data at 77K. In all cases, except $YbCl_3$ (see Appendix C) the pressure was cycled at least once to check for hysteresis. None was ever observed.

D. Experimental Results

Raw data for the ^{35}Cl resonance in the hexagonal trichlorides as a function of pressure is presented in Appendix B. The data was analyzed by least squares methods (Barford, 1967) according to the equation

$$\nu(P) = \nu_0 + mP \qquad (3.1)$$

where m is $(\partial\nu/\partial P)_T$. In all cases m is negative and independent of pressure over the range of pressures used. The results at 77K are summarized in Table 3.1. ν_Q is the pure quadrupole frequency measured at one atmosphere. The uncertainty in ν_Q is the standard deviation of at least five separate measurements. ν_0 and $(\partial\nu/\partial P)_T$ are obtained from the least squares fit to the raw data. The uncertainties here are statistical best estimates of error. The normalized pressure coefficient $\nu_0^{-1}\,(\partial\nu/\partial P)_T$ is calculated from ν_0 and $(\partial\nu/\partial P)_T$. It is plotted with respect to compound in Figure 3.3.

Table 3.1. Summary of Frequency versus Pressure Data at 77K

Compound	ν_Q(kHz)	ν_o(kHz)	$(\partial\nu/\partial P)_T$ (Hz/psi)	$\nu_o^{-1}(\partial\nu/\partial P)_T$ (10^{-6} cm^2/kg)
$CeCl_3$	4377.2 ± 0.3	4378.6 ± 0.3	-1.720 ± 0.006	-5.586 ± 0.020
$PrCl_3$	4561.9 ± 0.8	4562.4 ± 0.4	-1.648 ± 0.007	-5.136 ± 0.023
$NdCl_3$	4722.3 ± 0.3	4723.0 ± 0.2	-1.592 ± 0.006	-4.794 ± 0.018
$SmCl_3$	5026.8 ± 0.5	5027.1 ± 0.4	-1.503 ± 0.011	-4.252 ± 0.031
$GdCl_3$	5307.6 ± 0.3	5308.5 ± 0.2	-1.439 ± 0.006	-3.855 ± 0.016

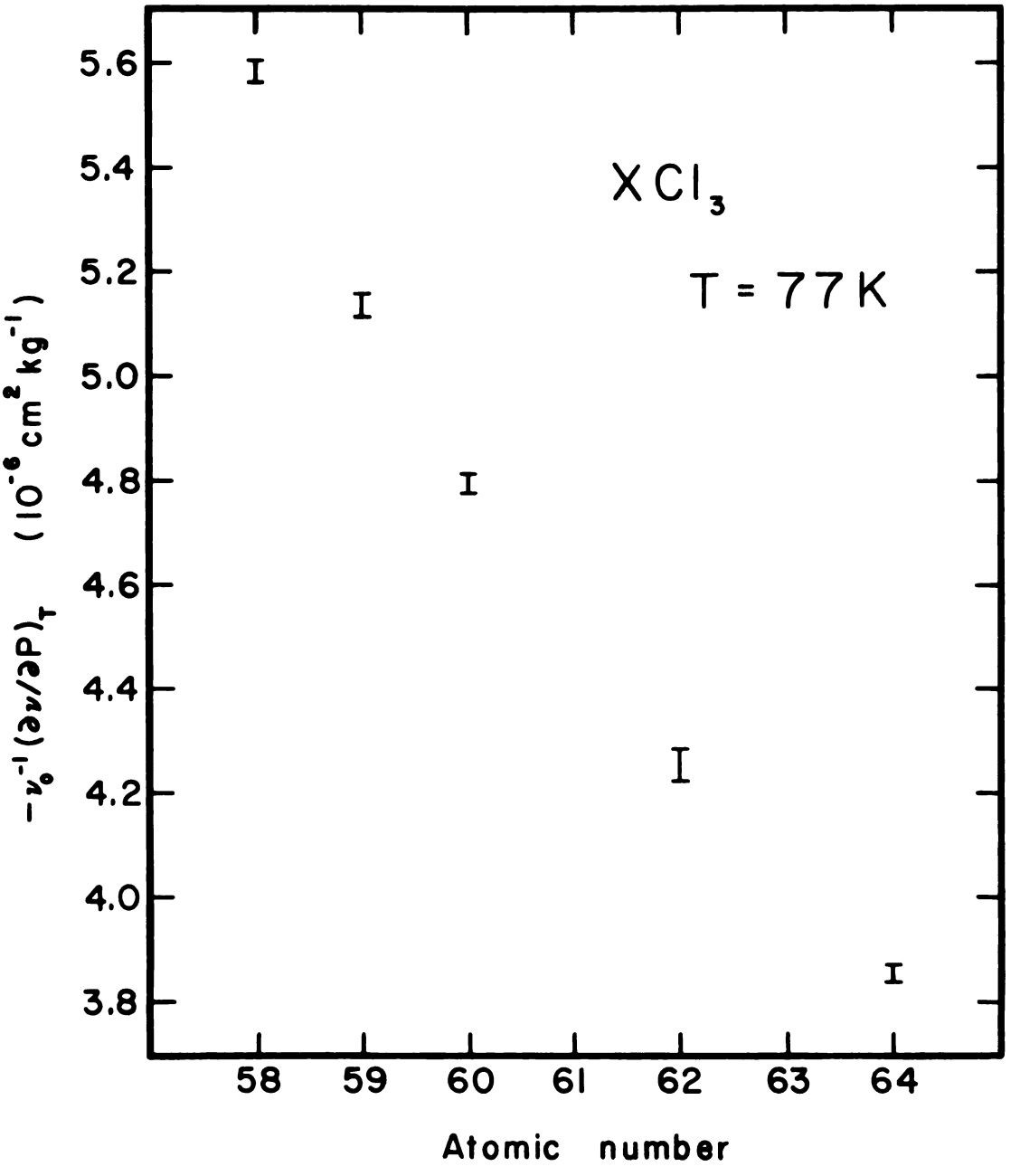

Figure 3.3. Normalized Pressure Coefficient of Quadrupole Frequency versus Atomic Number

IV. THEORY

A. Introduction

The calculation of electric field gradients in ionic solids is a complicated quantum mechanical problem. Since the necessary many-ion wave functions are not known, the usual procedure is to assume an appropriate two-ion model for the field gradient and then sum the contribution from each ion in the crystal. Once the two-ion model has been chosen, the calculation of the electric field gradient becomes a geometrical problem.

We define the normalized pressure coefficient of the quadrupole frequency as

$$\nu_o^{-1}(\partial\nu/\partial P)_T = -\beta[\partial(\nu/\nu_o)/\partial(V/V_o)]_T \qquad (4.1)$$

where ν_o and V_o are the frequency and unit cell volume at zero pressure. The bulk compressibility, β, is given by

$$\beta = -V_o^{-1}(\partial V/\partial P)_T = \alpha_1 + \alpha_2 + \alpha_3 \ . \qquad (4.2)$$

The three linear compressibilities along the crystallographic axes are α_1, α_2 and α_3. For hexagonal crystals, symmetry requires that $\alpha_1 = \alpha_2$. In order to properly calculate the dependence of the quadrupole frequency on cell volume it is necessary to know the compressibility ratio $r = \alpha_3/\alpha_1$ as a function of pressure. We consider this point in Section B along with the bulk compressibility. In addition it is essential to have information concerning the variation of the chloride positional parameters with pressure. However

no experimental data is available and we assume that they are independent of pressure.

In Section C we briefly discuss previous attempts to calculate electric field gradients in solids in the two-ion approximation. In Section D we introduce the soft sphere model used in this work, and present the results of calculations of quadrupole frequencies and asymmetry parameters for all of the hexagonal rare earth trichlorides. Finally in Section E we combine the results of Sections B and D to calculate normalized pressure coefficients from the soft sphere model and compare these calculations with the experimental results.

B. Compressibility of $LaCl_3$

The best and most complete information on the compressibility in these compounds would be a full X-ray measurement of the lattice constants and positional parameters as a function of pressure and temperature. Such experiments are difficult and have not been performed. Indeed even the bulk compressibility has not been measured. The only piece of evidence on the elastic behavior in these compounds appears to be a recent paper by Stedman and Newman (1971) in which the elastic constants, C_{ij}, of $LaCl_3$ are calculated from optical data.

Stedman and Newman give three sets of elastic constants and label them A, B and C. They are reproduced here as part of Table 4.1. The different sets result from different assumptions concerning the nature of the bonds in $LaCl_3$, but all are derived by assuming Hooke's Law forces between ions.

This model seems questionable to us for two reasons. First it requires attractive forces between chloride ions, and second it attempts to derive information about the long wavelength acoustic phonons from the behavior of the optical phonons.

These objections not withstanding, the lack of experimental data on the elastic behavior of these compounds forces us to examine the results of Stedman and Newman in some detail. It is possible to calculate the compressibility of a crystal from a knowledge of the elastic constants. For a general review of this topic see Hearmon (1946). The linear compressibilities are usually written in terms of the elastic compliance constants, S_{ij},

$$\alpha_i = \sum_{j=1}^{3} S_{ij} \quad , \qquad i = 1, 3 \quad . \tag{4.3}$$

The compliance constants are related to the elastic constants by (Cady, 1964)

$$\sum_{k=1}^{6} S_{jk}C_{kj'} = \sum_{k=1}^{6} C_{jk}S_{kj'} = \delta_{jj'} \quad . \tag{4.4}$$

For hexagonal systems it is a straightforward matter to solve Eq. (4.4) for S_{ij} in terms of C_{ij} and substitute the result into Eq. (4.3). In terms of the elastic constants the linear compressibilities are given by

$$\alpha_1 = \alpha_2 = (C_{33} - C_{13})/D \tag{4.5}$$

and

$$\alpha_3 = (C_{11} + C_{12} - 2C_{13})/D \tag{4.6}$$

where

$$D = C_{33}(C_{11} + C_{12}) - 2C_{13}^2 \qquad (4.7)$$

The compressibilities calculated in this way from the data of Stedman and Newman are presented as part of Table 4.1. They seemed to us to be rather small.

In order to examine the validity of these elastic constants we have calculated the Debye temperature that results from them (Carlson, Current and Foiles, 1971). In $LaCl_3$ the Debye temperature, Θ_D, has been calculated from low temperature specific heat data to be 149.5±1.5 K (Varsanyi and Maita, 1965). Betts, Bhatia and Horton (1956) derive three approximate formulae for calculating Θ_D as a function of elastic constants for hexagonal systems. Wolcott (1959) gives a set of numerical tables. Using these four methods, we have calculated Θ_D from each of the sets of C_{ij} of Stedman and Newman. The results for the second method of Betts, Bhatia and Horton appear in Table 4.1 along with some data on other compounds for comparison. There is good agreement among the four methods. However the calculated Debye temperatures are from three and one-half to four times larger than the measured value. We are therefore forced to conclude that the elastic constants of Stedman and Newman are in error.

The following argument is used to estimate the size of this error. The Debye temperature is proportional to the mean sound velocity, which for hexagonal systems is given by (Wolcott, equation 6)

$$v_m = f\sqrt{C_{44}/\rho} \qquad (4.8)$$

Table 4.1. Elastic Constants, Compressibilities and Debye Temperatures for Selected Materials

	C_{11}[a]	C_{12}[a]	C_{13}[a]	C_{33}[a]	C_{44}[a]	α_1[b]	α_3[b]	$r=\alpha_3/\alpha_1$	β[b]	β[d]	$\Theta_D(K)$[c]	$\Theta_D(K)$[d]
$LaCl_3$(A)[e]	3.065	1.238	1.653	3.611	1.677	0.194	0.099	0.509	0.488	---	593.9	149.5
$LaCl_3$(B)[e]	2.585	1.670	1.517	3.419	1.731	0.191	0.123	0.642	0.496	---	513.6	149.5
$LaCl_3$(C)[e]	2.952	1.564	1.607	3.648	1.742	0.181	0.115	0.638	0.467	---	570.3	149.5
Beryl[f]	2.692	0.964	0.669	2.372	0.654	0.210	0.287	1.368	0.707	0.53[k]	---	---
NaCl[g]	0.486	0.127	---	---	0.128	---	---	---	3.98	3.8	298	308
KCl[g]	0.400	0.062	---	---	0.062	---	---	---	5.61	4.8	241	230
AgCl[h]	0.600	0.360	---	---	0.062	---	---	---	2.23	---	154	180

[a]Units of 10^{12} dyne/cm^2.

[b]Units of 10^{-6} cm^2/kg. Calculated from C_{ij}.

[c]Calculated from Betts, Bhatia and Horton (1956) using eqn 6.2.

[d]Measured value.

[e]Stedman and Newman (1971).

[f]Hearmon (1946), $3BeO \cdot Al_2O_3 \cdot 6SiO_2$.

[g]Experimental data from Kittel (1956). Cubic material.

[h]Elastic constants from Kittel (1956) and Θ_D from Gopal (1966). Cubic material.

[k]Bridgman (1928).

where ρ is the density and f is a numerical function of ratios of the other elastic constants. By examining Wolcott's tables, we conclude the f is slowly varying. If we assume that the relative sizes of the C_{ij}'s of Stedman and Newman are approximately correct, then we are forced to conclude that their magnitudes are too large by a factor of from 12 to 16. Based on this argument we estimate that β for $LaCl_3$ is somewhere between 6 and 8 x 10^{-6} cm^2/kg. If the simple scaling argument is not valid, this estimate could be off by as much as a factor of two or three. Based on the values of β for other chloride salts, our personal feeling is that the estimate is probably too large rather than too small. As far as the ratio of linear compressibilities is concerned, we have assumed a value somewhere between 0.4 and 0.7, but stress the fact that this choice is almost completely arbitrary. Certainly a good experimental determination of these numbers is needed.

C. The Point Charge Model

In the point charge model of electric field gradients one assumes that each ion in the crystal can be represented by a spherical charge distribution having negligible overlap with other ions. One then replaces this spherical distribution by an appropriate point charge located at the nuclear position. The contribution to the field gradient from each ion is summed over the entire crystal:

$$q_{sum} = \sum_{\alpha} 2z_{\alpha}/R_{\alpha}^3 \quad , \qquad (4.9)$$

where R_{α} is the distance to the ion α and z_{α} is its charge.

In performing this sum the contribution of each ion must be rotated into a common coordinate system. Details are presented in Appendix D.

A closed shell ion such as Cl^- has a spherical electronic charge distribution which produces no field gradient at the nucleus. However if such an ion is placed in an external field gradient the electronic charge distribution is distorted. This distortion produces an additional contribution to the field gradient at the nucleus which is proportional to the externally applied gradient. The ratio between the gradient produced by distortion and the external gradient is called the Sternheimer antishielding factor (γ_∞). It has been calculated by Sternheimer (1956) and others (Lucken, 1969, p. 90). Sternheimer's result is $\gamma_\infty = -56.6$. The net field gradient at the nucleus is then

$$q_p = (1 - \gamma_\infty) q_{sum} . \qquad (4.10)$$

Burns and Wikner (1961) have calculated $\gamma_\infty = -27$ for Cl^- using contracted wavefunctions which they claim are representative of Cl^- in solids. Attempts to fit the point charge model to the observed quadrupole frequencies in various solids usually result in antishielding factors of from -10 to -40.

Point charge calculations for some of the hexagonal rare earth trichlorides have been reported by Carlson and Adams (1969). They found $(1 - \gamma_\infty) = 15.4$ necessary to fit the observed frequency in $LaCl_3$. With this same value of the antishielding parameter the calculated frequency in $GdCl_3$ is too low. In addition the asymmetry parameters are poorly predicted.

We have carried out point charge calculations for all of the hexagonal rare earth trichlorides using the structure data discussed previously. We have chosen $(1 - \gamma_\infty) = 17.59$ so as to fit the observed frequency in $GdCl_3$. The results for all compounds are given in Appendix D in Table D.1. The frequencies and asymmetry parameters are plotted with respect to compound in Figures 4.2 and 4.3 in the next section.

D. The Soft Sphere Model of Electric Field Gradients

Consider two closed shell ions, e.g. K^+ and Cl^-, separated by a large internuclear distance. It is assumed that the field gradient at the chloride nucleus is correctly described by the point charge model together with the theoretical antishielding parameter. As the ions are moved together it is clear that the point charge model must eventually fail. The ions no longer see each other as point charges, but as distributions of charge which become nonspherical as the outer parts of ions come into contact and distort each other.

Several authors have stressed the need for including an overlap contribution to the gradient. Das and Karplus (1959) suggested that a contribution to the gradient proportional to the overlap integral between ions in the KCl molecule was necessary to fit the experimental data. In a later paper (Das and Karplus, 1965) they performed such a calculation and showed that the overlap effect was important. Several papers (Taylor, 1968; Sawatsky and Hupkes, 1970; Sharma, 1970; Sharma, 1971) have dealt with the same effects in Al_2O_3, Cr_2O_3 and Fe_2O_3.

In the paragraphs that follow we will discuss a systematic method of introducing such overlap effects into field gradient calculations. We first discuss a Hartree-Fock, self-consistent field (HF-SCF) calculation by Matcha for the KCl molecule. From this calculation we deduce a functional form for the overlap contribution to the chloride field gradient. We then discuss a paper by Gilbert on the Born-Meyer repulsive potential between closed shell ions and use the results of a Hartree-Fock-Slater (HFS) calculation of ionic wavefunctions to extend Gilbert's work to other ions. Finally we introduce the soft sphere model of electric field gradients and discuss its application to the hexagonal rare earth trichlorides. This section concludes with some comments on the limitations of the model and its application to other crystal structures.

Matcha has recently calculated various molecular properties of alkali halide molecules using HF-SCF wavefunctions. In one paper (Matcha, 1970) he considers KCl and presents results for the gradient at the chloride nucleus for several internuclear separations. His results are summarized in Table 4.2.

Table 4.2. KCl Molecule after Matcha

R(bohr)	4.300	4.700	5.039	5.300	5.650
q_{Cl}(bohr^{-3})	-0.76931	-0.37517	-0.10043	0.06069	0.18729

At the equilibrium separation of the molecule (R = 5.039 bohr) the measured field gradient is ±0.003 bohr^{-3} (Ramsey, 1956). The point charge model alone (with γ_∞ = -56.6) gives q = 0.89 bohr^{-3}.

Das and Karplus (1965) obtain values for q between 0.33 and 0.13 $bohr^{-3}$ when they include some effects of molecular overlap. Matcha's result of $q = -0.10$ $bohr^{-3}$ represents substantial improvement over the above. In addition Matcha's calculations allow us to examine the dependence of q on internuclear separation.

We decompose Matcha's results into two parts, one due to the point charge contribution and the other due to the wavefunction distortion caused by orbital overlap. The overlap contribution is then

$$q_o = q - 2(1 - \gamma_\infty)/R^3 = q - q_p \ , \qquad (4.11)$$

where q is Matcha's calculated value and γ_∞ is -56.6. For the three largest separations calculated by Matcha we find

$$q_o = B \exp[-R/\rho], \qquad (4.12)$$

with $B = -752.0$ $bohr^{-3}$ and $\rho = 0.7594$ bohr. In Figure 4.1, q, q_p and q_o are plotted with respect to internuclear separation. The exponential dependence of the overlap contribution to the electric field gradient seems reasonable to us. Since the ion distortion is a function of the molecular overlap integral, it should fall off rapidly with increasing separation. We would expect that the parameter ρ is in some way characteristic of the "softness" on an ion pair.

In attempting to parameterize these ideas we were lead to a paper by Gilbert (1968) which proposed an extension of the Born-Meyer repulsive interaction between closed shell

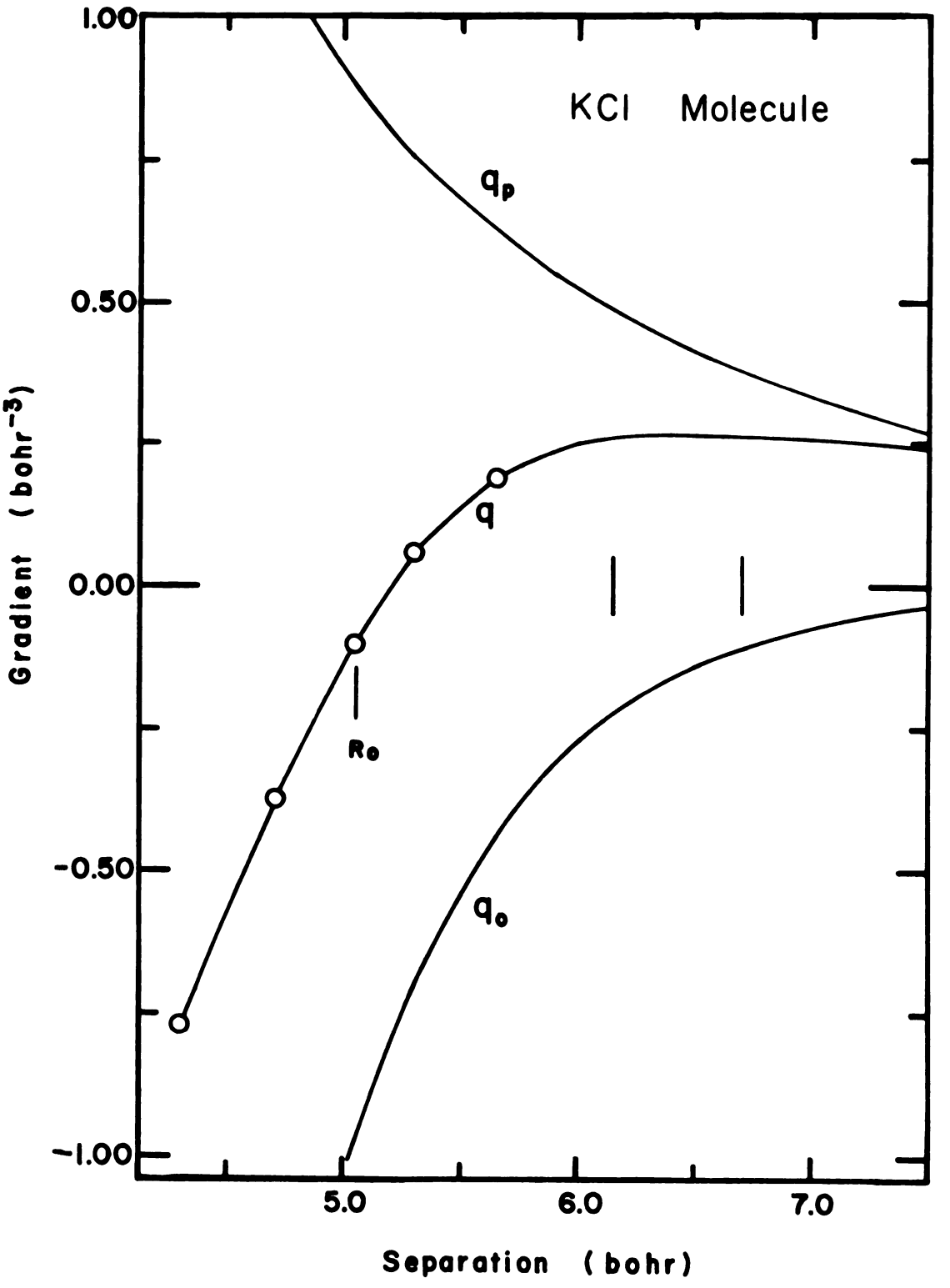

Figure 4.1. Electric Field Gradient at the Chloride Nucleus in the KCl Molecule

ions. Gilbert writes the interaction energy between ions i and j as

$$U_{ij} = f\ \rho_{ij}\ \exp[(R_{ij} - R)/\rho_{ij}], \qquad (4.13)$$

where R_{ij} and ρ_{ij} are characteristic radii and softness* parameters for the ion pair, and f is a standard force. From spectroscopic data for alkali halide monomers Gilbert deduces the additivity rules $R_{ij} = R_i + R_j$ and $\rho_{ij} = \rho_i + \rho_j$, where R_i and ρ_i are parameters for individual ions. From the same spectroscopic data he has assigned values to individual ion parameters. These are listed as part of Table 4.3.

In trying to extend to other ions the meaning of Gilbert's parameters we have carried out a series of calculations of ionic wavefunctions using the HFS method. We used a computer program originally written by Herman and Skillman (1963). A working copy of the program was kindly provided by Dr. D.Y. Smith of Argonne National Laboratory. We have observed a correlation for alkali ions between the radii quoted by Gilbert and the natural logarithm of electronic charge density calculated by HFS. In addition the variation of the charge density is nearly exponential near Gilbert's value of radius.

We define an HFS softness parameter by

$$\rho(\mathrm{HFS}) = -\ \Delta R/\Delta(\ell n \rho_s)\ , \qquad (4.14)$$

where ρ_s is the electronic charge density from HFS and the slope is evaluated at Gilbert's value of R. For the alkali

---

*Earlier workers have called ρ a hardness parameter. We prefer Gilbert's characterization since a larger value of ρ implies a softer repulsive force.

ions $\ell n\rho_s$ seems to be consistently near -4.3. The results are more obscure for the halide ions. Gilbert's parameters along with those deduced from the HFS calculation are presented in Table 4.3.

We define radii and softness parameters for metal ions from the HFS calculation. The parameters are evaluated where the natural logarithm of the electronic charge density is -4.3000. The values of R_i and ρ_i for various ions of interest in this work are presented in Table 4.4. The residual charge outside a sphere of radius R_i is of the order of one electron. Note that the halide radii are considerably smaller than those of Gilbert.

We define the electric field gradient at ion i in the soft sphere model as

$$q_i = \sum_{j \neq i} (q_p^j - q_o^j) \ , \qquad (4.15)$$

where the sum runs over all ions in the crystal. The point charge contribution is given by

$$q_p^j = 2 \ z_j(1 - \gamma_i)/R^3 \ , \qquad (4.16)$$

where R is the distance from ion i to ion j with charge z_j. The antishielding factor for ion i is treated as a free parameter. For Cl^- we expect its value to be somewhat less than the theoretical free ion value, since a chloride ion constrained in a potential well will certainly polarize less in response to an external gradient than a free ion. The overlap contribution is given by

$$q_o^j = F \exp[(R_{ij} - R)/\rho_{ij}] \ . \qquad (4.17)$$

Table 4.3. Ionic Parameters after Gilbert

Ion	R(Gilbert)[a]	ρ(Gilbert)[a]	$\ln\rho_s(R = R_G)$	ρ(HFS)[b]
Li^+	1.31	0.131	-4.34	0.205
Na^+	1.80	0.150	-4.33	0.163
K^+	2.35	0.200	-4.28	0.338
Rb^+	2.59	0.217	-4.35	0.369
Cs^+	2.87	0.245	-4.28	0.417
F^-	2.59	0.338	-5.10	0.470
Cl^-	3.59	0.449	-5.89	0.585
Br^-	3.90	0.488	-6.08	0.619
I^-	4.37	0.546	-6.31	0.660

[a]Values in bohrs taken from Gilbert (1968).

[b]Values in bohrs from HFS calculations.

Table 4.4. Ionic Parameters from HFS

Ion	R(bohr)	ρ(bohr)	Residual Charge[a]
Li^+	1.306	0.2047	0.08
Na^+	1.801	0.2481	0.17
K^+	2.361	0.3304	0.36
Rb^+	2.590	0.3690	0.52
Cs^+	2.880	0.4176	0.73
F^-	2.230	0.4172	0.64
Cl^-	2.740	0.4947	1.01
Br^-	2.896	0.5277	1.20
I^-	3.140	0.5803	1.50
La^{3+}	2.636	0.3267	0.42
Ce^{3+}	2.608	0.3204	0.42
Pr^{3+}	2.581	0.3148	0.40
Nd^{3+}	2.556	0.3096	0.37
Pm^{3+}	2.531	0.3048	0.38
Sm^{3+}	2.507	0.3004	0.36
Eu^{3+}	2.484	0.2962	0.34
Gd^{3+}	2.462	0.2923	0.32

[a]Charge in units of e outside characteristic radius.

The additivity rules for the soft sphere parameters are assumed to hold. We treat F as a free parameter and restrict the overlap contribution to near neighbors ($R \leq 4.0$ Å). The soft sphere parameters for metal ions are taken from HFS calculations. We discuss three possible choices of parameters for Cl^- below.

In what we call data set A we choose the chloride parameters directly from the HFS calculation. This gives $R_{Cl} = 2.740$ bohr and $\rho_{Cl} = 0.4947$ bohr. Since F and R_{Cl} are not independent parameters (the quantity $F \exp(R_{Cl}/\rho_{ij})$ enters for all ions) we fix R_{Cl} at this value. For data set B we return to the Matcha calculation which indicates a combined softness for K^+ plus Cl^- of 0.7594 bohr. By subtracting the HFS value for K^+ we obtain a softness for Cl^- of 0.4290 bohr. For data set C we arbitrarily choose $\rho_{Cl} = 0.4000$ bohr. For each set we then adjust the free parameters F and $(1 - \gamma_\infty)$ so as to fit the observed quadrupole frequency and asymmetry parameter in $GdCl_3$. The parameters for the three data sets are listed in Table 4.5. With these parameters we then calculate the electric field gradient for each of the other hexagonal rare earth trichlorides.

Table 4.5. Parameters for $GdCl_3$: Soft Sphere Model

Set	R_{Cl}(bohr)	ρ_{Cl}(bohr)	F(bohr^{-3})	$(1 - \gamma_\infty)$
A	2.740	0.4947	0.4346	28.25
B	2.740	0.4290	0.5695	30.95
C	2.740	0.4000	0.6710	32.99

The detailed results are tabulated in Appendix D, and the values of quadrupole frequency and asymmetry parameter are plotted with respect to compound in Figures 4.2 and 4.3.

The agreement with the experimental values is quite good. For set B the computed values of ν are within 2.5% of the experimental values for all compounds, while η for $PrCl_3$ is calculated to within 0.5% of the measured value. The substantial improvement over the point charge model should be noted. There is still room for improvement however, since the variation of frequency with compound is not quite right from $LaCl_3$ to $NdCl_3$. None of the three sets gives a fast enough increase in frequency as ones goes from $LaCl_3$ to $NdCl_3$.

Two other attempts to fit the experimental data within the context of this model were made. While not resulting in a good fit they serve to illustrate some useful points. First, if the Gilbert radius for Cl^- is used the gradient is completely dominated by the near neighbor chlorides. The amount of overlap required to reduce the frequency and asymmetry parameter to their experimental values in $GdCl_3$ is sufficient to cause the gradient tensor to be in the wrong direction. That is, in its principal axis system, the smallest element (V_{xx}) is not along the c-axis as it should be. The second point involves the use of the full anti-shielding parameter for the free Cl^- ion. We assumed the HFS values for the Gd^{3+} soft sphere parameters and set F = 1.0 and $(1 - \gamma_\infty) = 57.6$. We then varied the chloride parameters

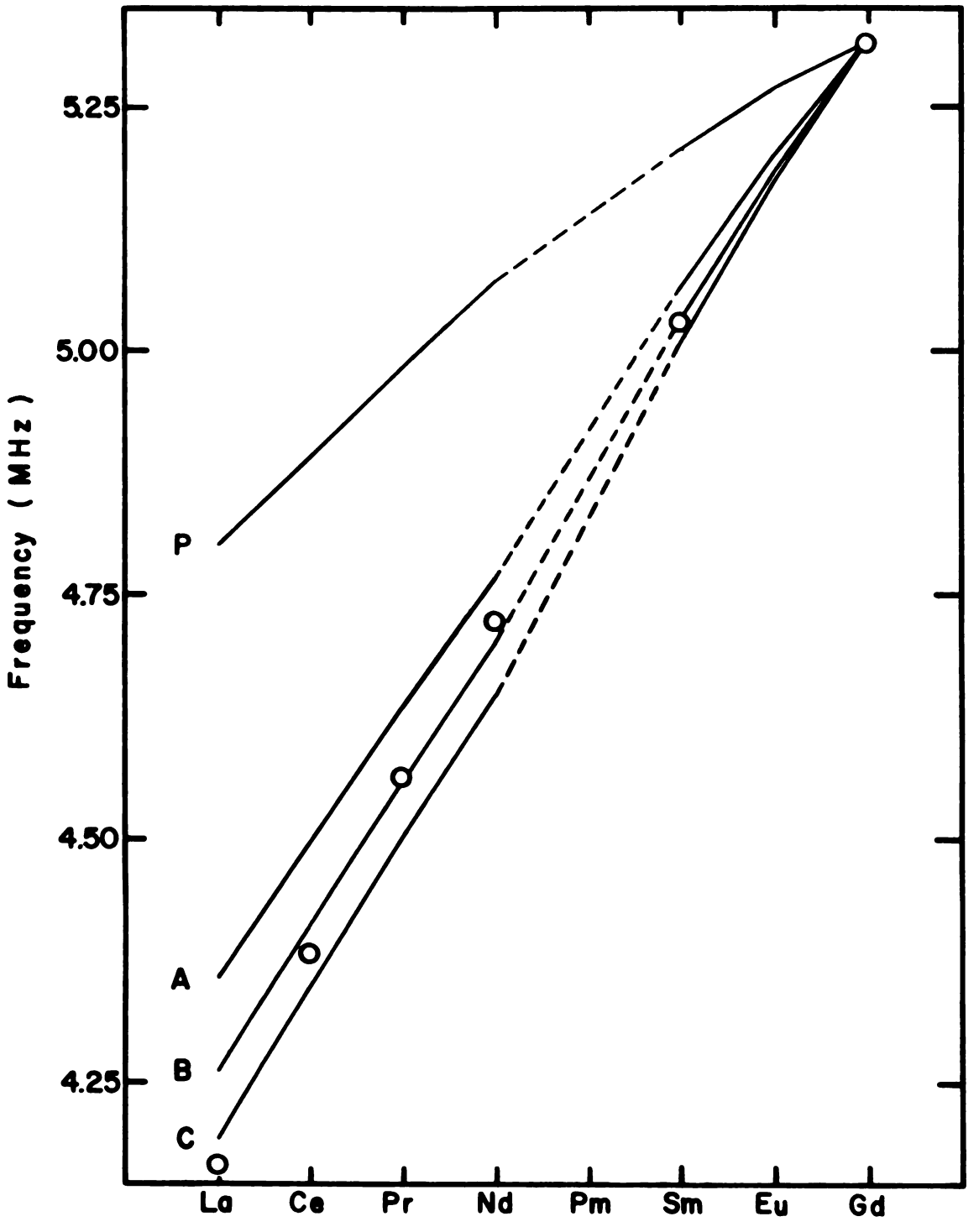

Figure 4.2. Quadrupole Frequency versus Compound

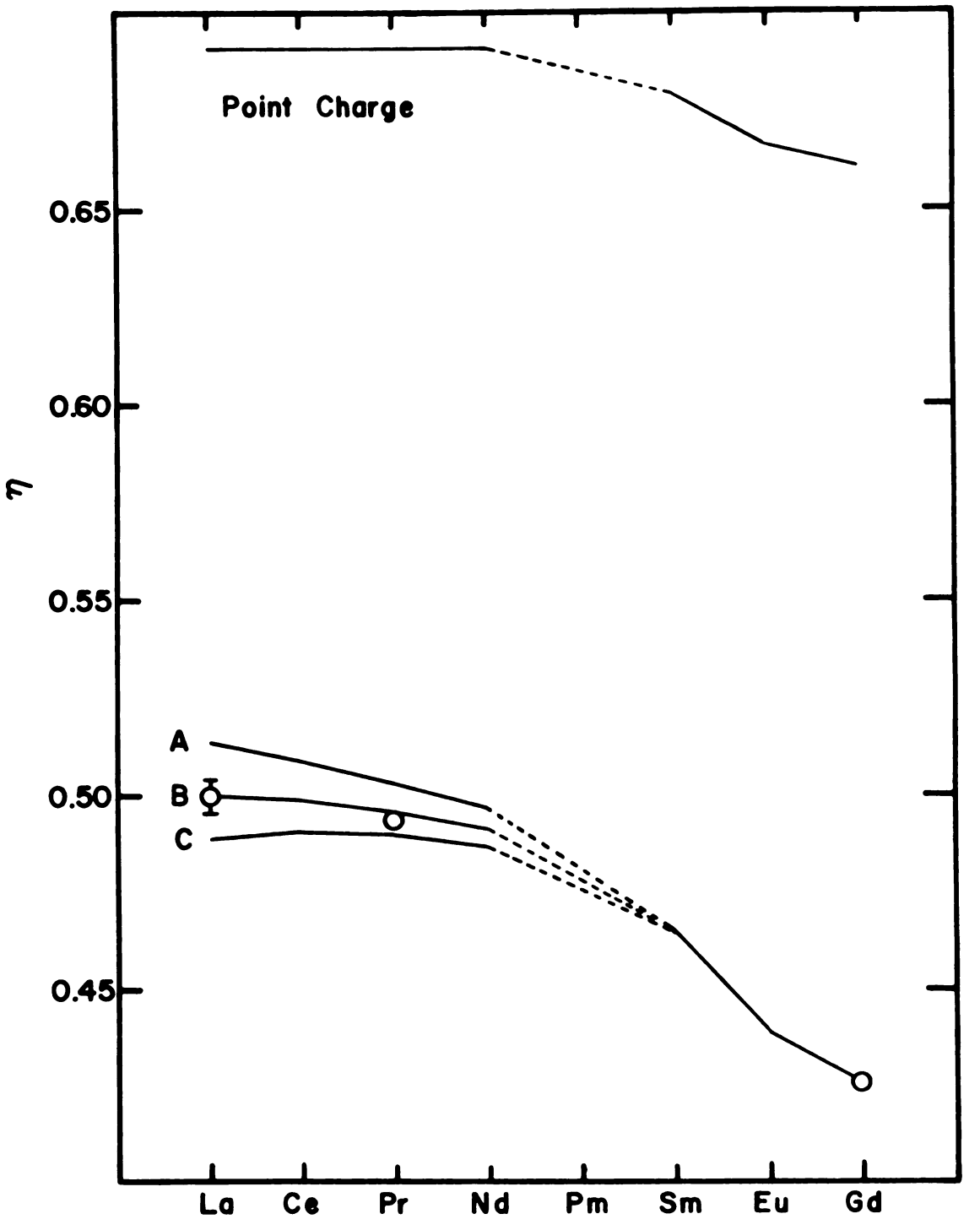

Figure 4.3. Asymmetry Parameter versus Compound

to fit the experimental data for $GdCl_3$. Using these chloride parameters and the same F and antishielding factor, we varied the Pr^{3+} soft sphere parameters to obtain a fit to the experimental data for $PrCl_3$. The resulting soft sphere parameters were both significantly less than those assumed for Gd^{3+}. This is contrary to both the HFS calculations and our intuition.

There are a number of effects we have neglected in this model. Some of them we expect to be partially included in the parameterization of our model and the others we expect to be small. Those partially included are the effects of polarization of the chloride ion at whose nucleus the calculation is carried out, and the contributions due to three-body forces. In addition to an external field gradient at a chloride nucleus there is also an electric field. This field makes some contribution to the polarization of the chloride electronic wavefunction which in turn produces a contribution to the gradient at the nucleus. The dipole polarizability of Cl^- is not well known, but we expect that at least part of this effect is included in the antishielding parameter. Many-body effects are certainly important, but we feel that they are at least partially included in our parameterization of the overlap contribution. In other chlorides with different geometries they may manifest themselves through changes in the overlap strength F or the antishielding parameter. We have completely neglected any dipole or higher moment contribution to the lattice sums. The largest of these effects

would be from the more easily polarizable Cl^- ions. But since they are symmetrically placed, their effect would largely cancel. In addition most of the gradient appears to originate from the three nearest metal ions which have very small polarizability.

A variation of this model has been applied by Carlson (1971) to $CsPbCl_3$. In this compound the overlap contribution to the electric field gradient at the chloride nuclei appears to originate entirely from two nearby Pb^{2+} ions. The crystal exists in two phases, one cubic with a single frequency and the other tetragonal with two frequencies. Carlson has used the Pb-Cl separation of 2.802 Å in the cubic phase as the sum of the characteristic radii and deduces F = 0.8098 $bohr^{-3}$ and $\rho_{Pb} + \rho_{Cl} = 0.546$ bohr from the two frequencies in the tetragonal phase. His relatively large value for F and small value for ρ partially result from his use of the free ion value for the Cl^- antishielding parameter.

E. Volume Dependence of the Electric Field Gradient

The calculation of the volume dependence of the electric field gradient is a straightforward procedure. The lattice constants of the unit cell are reduced in a systematic way and the field gradient is calculated for each set of lattice constants. Since the linear compressibility ratio $r = \alpha_3/\alpha_1$ is so poorly known we reduced the values of the lattice constants A and C in such a manner as to correspond to a wide range of values for r. We made calculations in $GdCl_3$ for the extreme values r = 0.0 and r = ∞ as well as for several intermediate values. The choice r = 0.0 corresponds

to holding the value of C fixed and allowing all of the volume reduction to occur by shrinkage of the crystal along the a-axis. The other extreme, $r = \infty$, corresponds to holding the value of A constant and allowing all of the volume reduction to occur by shrinkage along the c-axis. The choice $r = 1.0$ corresponds to an isotropic compression in which A and C both decrease at the same rate (constant C/A ratio).

The volume dependence of the quadrupole frequency in $GdCl_3$ for the point charge model is illustrated in Figure 4.4. The frequency and volume have both been normalized to their zero pressure values. For all positive values of r the frequency increases as the volume decreases. This is exactly the opposite of the observed behavior. For this reason we will restrict ourselves to a discussion of the volume dependence in the soft sphere model only.

In the soft sphere model the exponential dependence of the overlap contribution to the field gradient can result in a smaller gradient as ions are moved closer together. The volume dependence of the quadrupole frequency in $GdCl_3$ for the three data sets of the soft sphere model is illustrated in Figures 4.5, 4.6 and 4.7. Again we have performed the calculations for a wide range of values of r. The scale on each of these figures is the same so that comparisons among them can be made easily. Several comments are in order.

First, the volume dependence for each of the data sets of the soft sphere model changes drastically as a function of r. Compression along the c-axis alone ($r = \infty$) yields

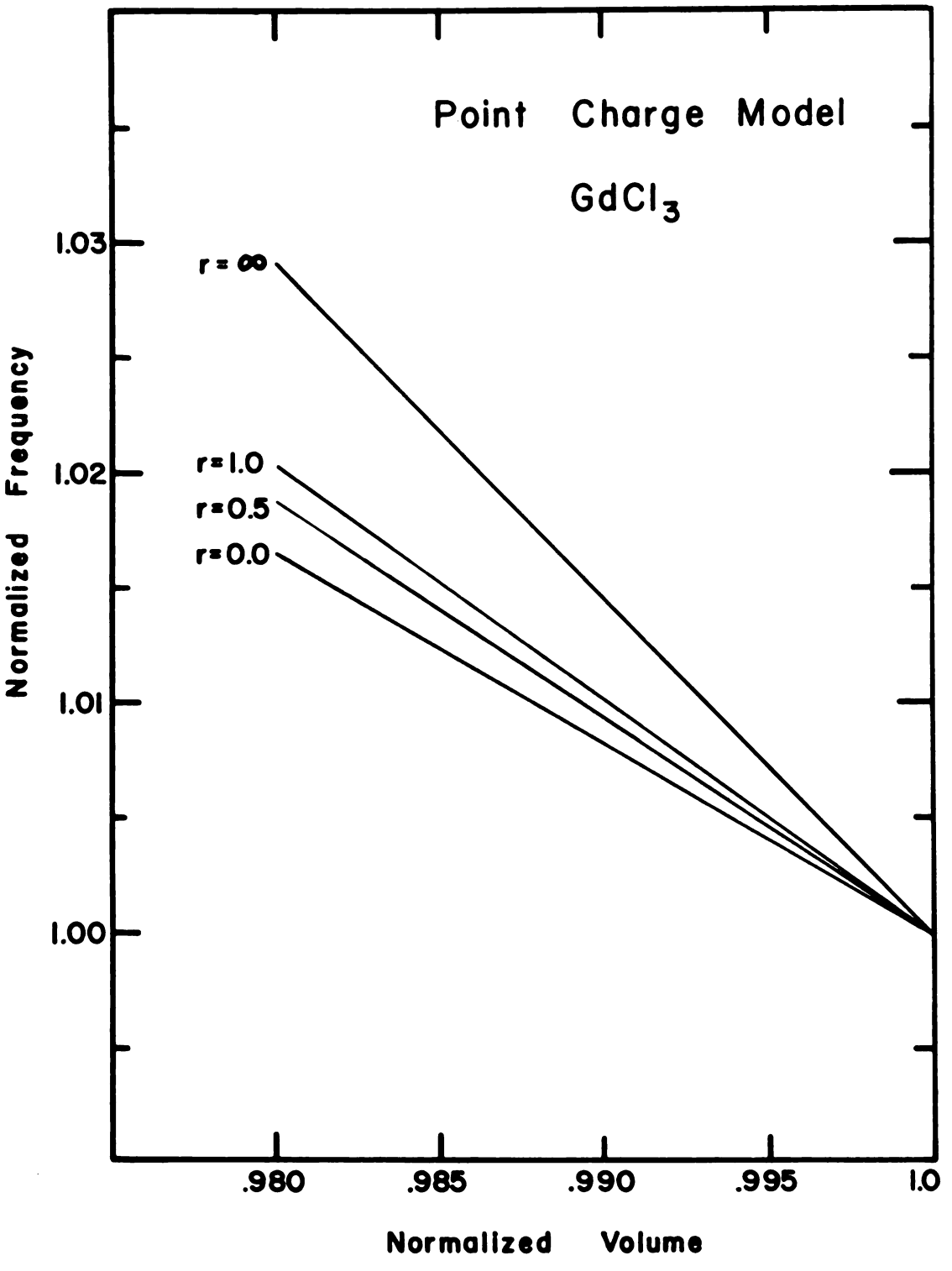

Figure 4.4. Quadrupole Frequency versus Volume in the Point Charge Model

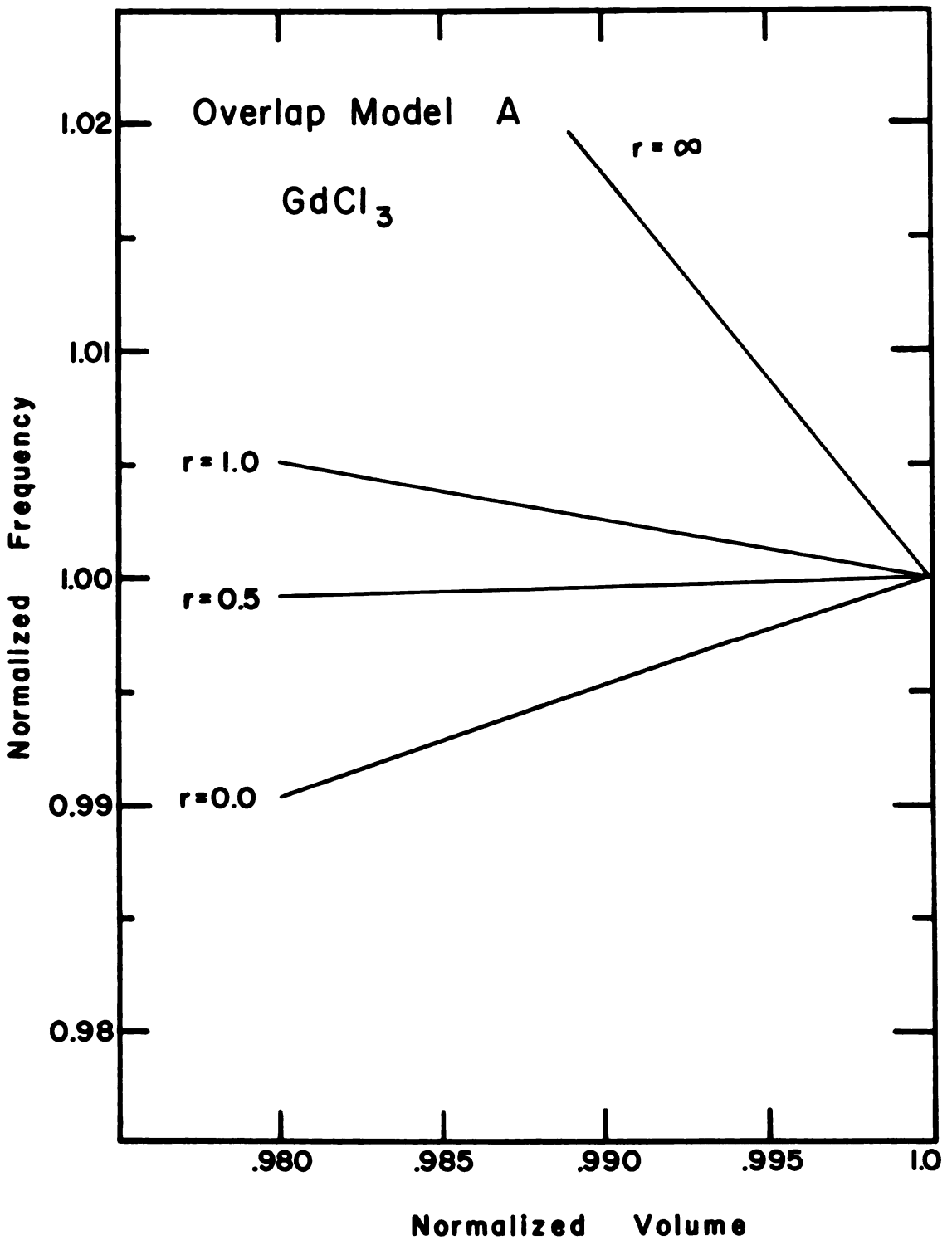

Figure 4.5. Quadrupole Frequency versus Volume in the Soft Sphere Model: Data Set A

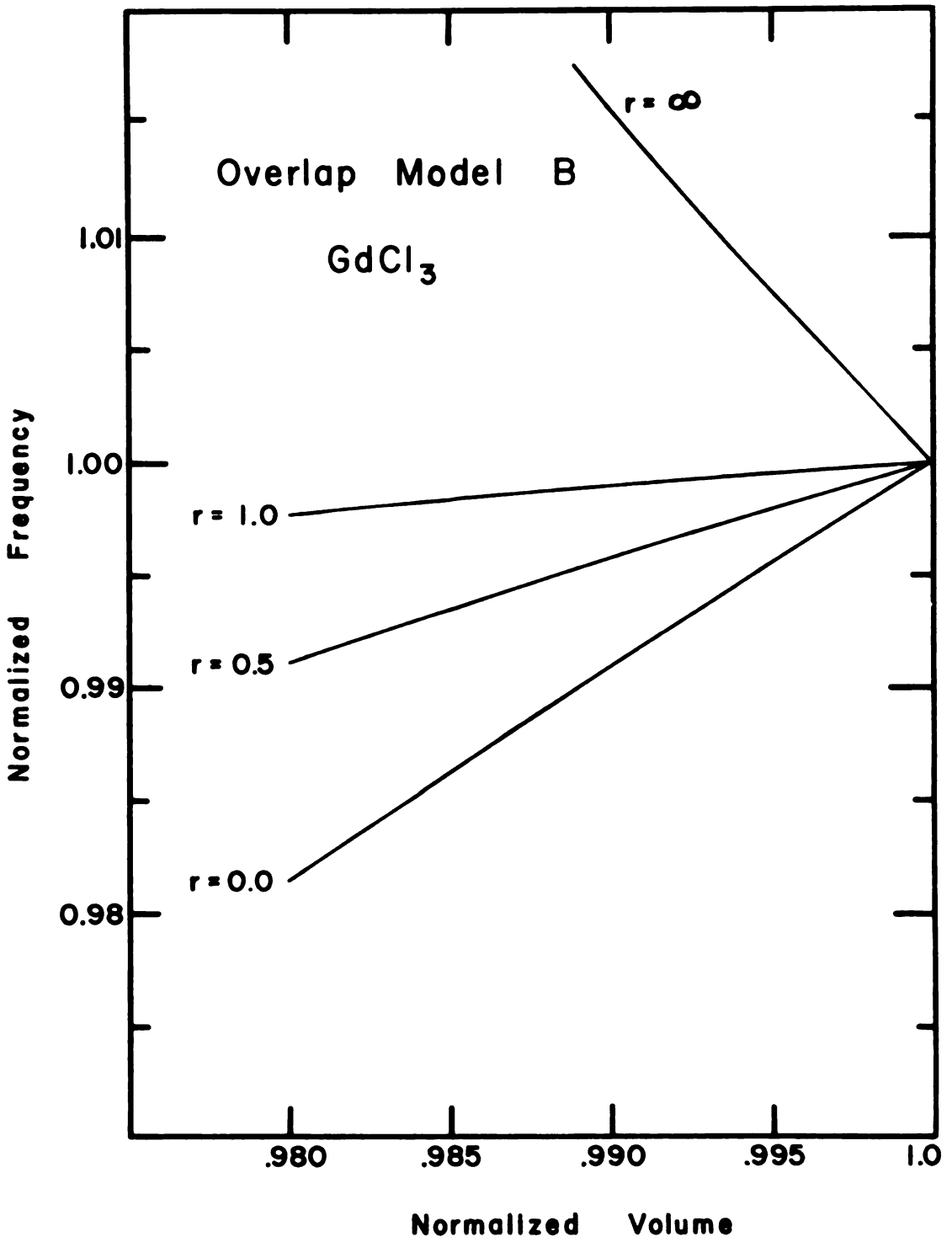

Figure 4.6. Quadrupole Frequency versus Volume in the Soft Sphere Model: Data Set B

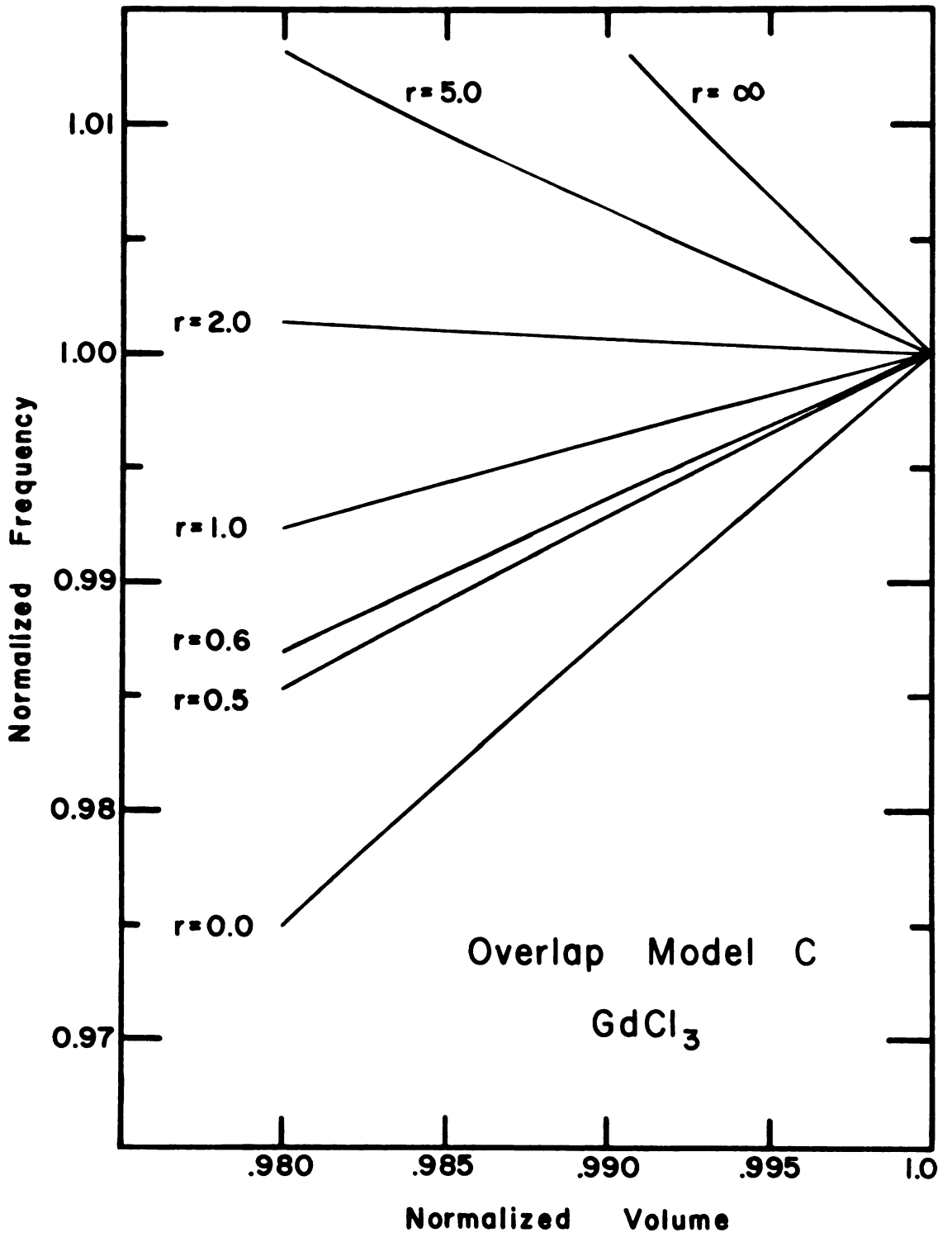

Figure 4.7. Quadrupole Frequency versus Volume in the Soft Sphere Model: Data Set C

frequencies which increase as the volume is decreased, while compression along the a-axis alone yields decreasing frequencies. Second, for a fixed value of r, $\partial\nu/\partial V$ decreases as one goes from data set A to data set C. This is easily understood, since data set C contains a larger overlap contribution to the field gradient than data set A. In a qualitative way one can consider the point charge component of the field gradient to contribute positive $\partial\nu/\partial V$ and the overlap component to contribute negative $\partial\nu/\partial V$. Finally, all of the curves are slightly non-linear; for $\partial\nu/\partial V$ negative they curve upward and for $\partial\nu/\partial V$ positive they curve downward. For r = 0.5 in data set B we tried to estimate whether or not this effect was observable. If we assume $\beta = 7 \times 10^{-6}$ cm^2/kg, then at a pressure of 5×10^3 kg/cm^2 (about 75,000 p.s.i.) the effect would produce a deviation from linearity in the frequency versus pressure curve (Figure B.5) of a few kHz. Since the uncertainty in frequency measurements is of the order of one kHz, we would not expect this possible non-linearity to be observable at the pressures achieved in this work. It is interesting to note that a distinct non-linearity was observed in $YbCl_3$ (Figure C.2). Unfortunately, as is pointed out in Appendix C, analysis of the field gradient in this compound must await better structural information.

We have calculated the volume dependence of the electric field gradient in the soft sphere model for all of the hexagonal rare earth trichlorides. We have arbitrarily limited

these calculations to values of r between 0.7 and 0.4. The elastic constants of Stedman and Newman (1971) seem to indicate a choice within this range, but our decision was based more on convenience than on belief in their numbers. The volume derivatives of the quadrupole frequency and asymmetry parameter of each compound for the three data sets of the soft sphere model are given in Table 4.6. All derivatives are evaluated at the zero pressure limit.

The normalized volume dependence of the quadrupole frequency in the soft sphere model is plotted with respect to compound in Figure 4.8. The three shaded areas in the figure correspond to the three different data sets of the soft sphere model. Each shaded area corresponds to choices of r between 0.7 and 0.4. For values of r outside this range the curves are similar. In order to compare these calculations with the experimentally measured normalized pressure coefficients, it is necessary to assume a value of the bulk compressibility for each compound. We have assumed $\beta = 7 \pm 1 \times 10^{-6}$ cm^2/kg for each compound and calculated an "experimental" value of $\partial(\nu/\nu_o)/\partial(V/V_o)$. These values are also plotted in Figure 4.8. The error bars attached to these values are a result of the assumed uncertainty in β and are somewhat arbitrary as discussed in Section B. A smaller value of β will result in an increase in the "experimental" value of $\partial(\nu/\nu_o)/\partial(V/V_o)$. In addition any variation of β from one compound to another will also shift these values.

Table 4.6. Results of Lattice Compression in the Soft Sphere Model

$r = \alpha_3/\alpha_1 = 0.7$	Data Set A		Data Set B		Data Set C	
Compound	$\frac{\partial(V/V_0)}{\partial(V/V_0)}$	$\frac{\partial n}{\partial(V/V_0)}$	$\frac{\partial(V/V_0)}{\partial(V/V_0)}$	$\frac{\partial n}{\partial(V/V_0)}$	$\frac{\partial(V/V_0)}{\partial(V/V_0)}$	$\frac{\partial n}{\partial(V/V_0)}$
$LaCl_3$	0.063	0.42	0.566	0.70	0.949	0.93
$CeCl_3$	0.047	0.45	0.533	0.71	0.902	0.93
$PrCl_3$	0.028	0.46	0.499	0.72	0.854	0.92
$NdCl_3$	0.015	0.48	0.473	0.73	0.817	0.93
$SmCl_3$	-0.043	0.51	0.366	0.76	0.672	0.92
$EuCl_3$	-0.070	0.54	0.320	0.78	0.610	0.95
$GdCl_3$	-0.095	0.56	0.278	0.80	0.553	0.96
$r = \alpha_3/\alpha_1 = 0.4$						
$LaCl_3$	0.201	0.50	0.731	0.90	1.135	1.23
$CeCl_3$	0.196	0.52	0.710	0.89	1.099	1.20
$PrCl_3$	0.188	0.53	0.687	0.89	1.063	1.17
$NdCl_3$	0.185	0.56	0.670	0.90	1.035	1.17
$SmCl_3$	0.148	0.60	0.581	0.92	0.904	1.14
$EuCl_3$	0.128	0.64	0.539	0.95	0.844	1.17
$GdCl_3$	0.107	0.66	0.500	0.98	0.790	1.18

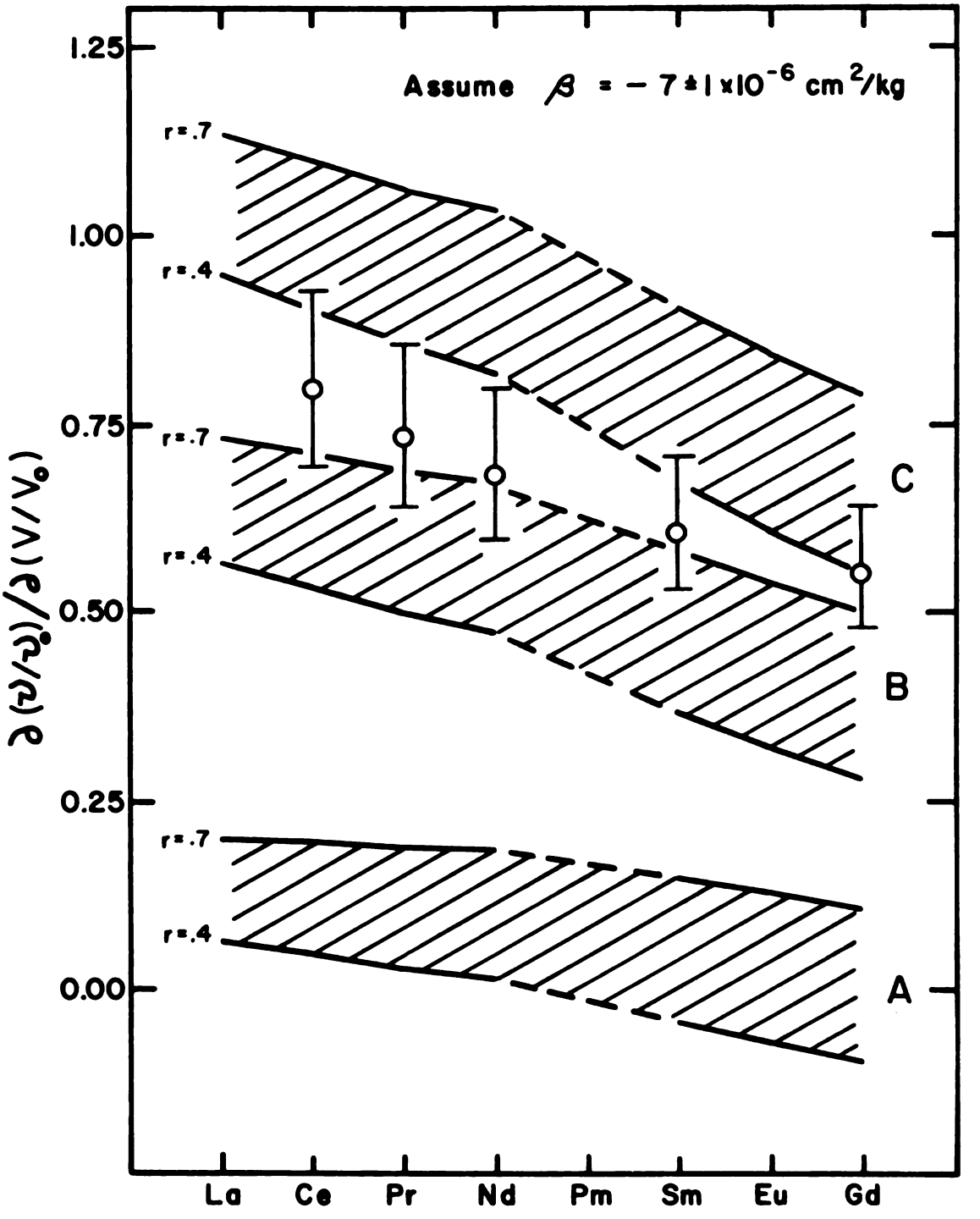

Figure 4.8. Derivative of Frequency with respect to Volume versus Compound in the Soft Sphere Model

There are several important comments that can be made about Figure 4.8. All of the calculated volume derivatives for each of the soft sphere data sets decrease as one goes from $LaCl_3$ to $GdCl_3$. This behavior is consistent with experiment. We might point out that in the point charge model the volume derivatives, in addition to being negative for all compounds and all positive values of r, increase slightly as one goes from $LaCl_3$ to $GdCl_3$. The "experimental" values fall on a smooth curve, but the calculated derivatives seem to have a kink at $NdCl_3$. We are unsure of the origin of this anomaly. We made a series of calculations in which we attempted to discover the effects of the experimental uncertainties in the lattice constants of $NdCl_3$ on the derivative of frequency with respect to volume. The effects of such structural uncertainties are totally invisible on the scale of Figure 4.8.

Because of our lack of information about β and r we are unwilling at this point to make a choice between data sets B and C. Data set A probably can be rejected as having too small an overlap contribution to the field gradient. We stress again that accurate values of bulk compressibilities and linear compressibility ratios in these compounds are essential to interpret the experimentally measured pressure dependence of the quadrupole frequency.

V. CONCLUSIONS

In introducing the soft sphere model of electric field gradients we have attempted to include in a systematic fashion the effects of wavefunction overlap. We have deduced a simple exponential dependence for the overlap contribution to the field gradient from HF-SCF calculations for the KCl molecule. We acknowledge the fact that in extending this idea from a diatomic molecule to a closely packed ionic solid, we are undoubtedly omitting important many-ion effects. We feel confident that future theoretical work will indicate a more comprehensive scheme for representing the overlap contribution.

We feel that representation of ions by a characteristic radius and softness parameter, which is an integral part of the soft sphere model, is an extremely useful idea. Using HFS calculations of ionic wavefunctions, we have made a connection between Gilbert's empirical parameters for alkali and halide ions, and parameters for other ions.

For the hexagonal rare earth trichlorides we have demonstrated that the soft sphere model of electric field gradients gives far better agreement with experiment than the earlier point charge model. The soft sphere model seems to indicate that the value for the Sternheimer antishielding parameter for Cl^- in these solids is about -30 as opposed to the theoretical free ion value of -56.6.

The pressure dependence of the quadrupole frequency in $CeCl_3$, $PrCl_3$, $NdCl_3$, $SmCl_3$ and $GdCl_3$ has been measured. It

is found that the frequency decreases linearly with increasing pressure in all compounds. For any physically reasonable value of the linear compressibility ratio, the point charge model when applied to these compounds predicts that the frequency should increase with pressure. This constitutes further evidence of the unsuitability of the point charge model. On the other hand the soft sphere model predicts that the frequency should decrease almost linearly with pressure, provided that the linear compression along the c-axis is slower than that along the a-axis. Future work should include a measurement of the geometrical changes in these compounds under pressure. The best method would be an x-ray measurement of the lattice constants and chloride positional parameters as a function of pressure. A direct measurement of the elastic constants would also be useful.

As soon as good crystal structure data is available for orthorhombic $TbCl_3$ and monoclinic $DyCl_3$, $HoCl_3$, $ErCl_3$, $TmCl_3$, $YbCl_3$, and $LuCl_3$, the model should be applied to these compounds. The monoclinic salts represent a severe change in geometry from the hexagonal salts, and a different value of the overlap strength may be necessary. However, we would expect the antishielding parameter to be roughly the same. In $TbCl_3$ one of the two chloride sites has an environment quite similar to that in the hexagonal salts. We expect that the soft sphere model will predict the frequency and asymmetry parameter well, using the same overlap strength and antishielding factor as in $GdCl_3$.

In conclusion we feel that the soft sphere model of electric field gradients in solids, by including the effects of molecular overlap, provides an important step forward in the theory of nuclear quadrupole resonance.

REFERENCES

REFERENCES

Barford, N.C., 1967, Experimental Measurements: Precision, Error and Truth, Addison-Wesley, London, p. 62.

Bersohn, Richard, 1958, J. Chem. Phys., 29, 326.

Bersohn, R. and Shulman, R.G., 1966, J. Chem. Phys., 45, 2298.

Betts, D.D., Bhatia, A.B. and Horton, G.K., 1956, Phys. Rev., 104, 43.

Bommer, H. and Hohmann, E., 1941, A. Anorg. Allgem. Chem., 248, 373.

Bridgman, P.W., 1928, Am. Jour. Sci., Fifth Series, 15, 287.

Brun, E. and Hofer, S.S., 1962, Z. Krist., 117, 37, 63.

Burns, Gerald and Wikner, E.G., 1961, Phys. Rev., 121, 155.

Cady, W.G., 1964, Piezoelectricity, Vol I, Dover Publications, New York.

Carlson, E.H., 1966, Bull. Am. Phys. Soc., 11, 377.

Carlson, E.H., 1969, Physics Letters, 29A, 696.

Carlson, E.H., 1971, J. Chem. Phys., to be published.

Carlson, E.H. and Adams, H.S., 1969, J. Chem. Phys., 51, 388.

Carlson, E.H., Current, D.H., and Foiles, C.L., 1971, submitted to J. Chem. Phys.

Das, T.P. and Hahn, E.L., 1958, Solid State Physics, Supplement I, edited by F. Seitz and D. Turnbull, Academic Press, New York.

Das, T.P. and M. Karplus, 1959, J. Chem. Phys., 30, 848.

Das, T.P. and Karplus, M., 1965, J. Chem. Phys., 42, 2885.

Garton, G., Hutchings, M.T., Shore, R. and Wolf, W.P., 1964, J. Chem. Phys., 41, 1970.

Gilbert, T.L., 1968, J. Chem. Phys., 49, 2640.

Gopal, E.S.R., 1966, Specific Heats at Low Temperatures, Plenum Press, New York.

Goree, W.S., McDowell, B., and Scott, T.A., 1965, Rev. Sci. Inst., 36, 99.

Hearmon, R.F.S., 1946, Revs. Modern. Phys., 18, 409.

Herman, F. and Skillman, S., 1963, Atomic Structure Calculations, Prentice-Hall, Englewood Cliffs, New Jersey.

Hessler, J.P., 1971, dissertation, The Low Temperature Cooperative Behavior of the Rare Earth Salts $GdCl_3$ and $PrCl_3$, Michigan State University.

Huges, W.E., Montgomery, C.G., Moulton, W.G. and Carlson, E.H., 1964, J. Chem. Phys., 41, 3470.

Kittel, C., 1956, Introduction to Solid State Physics, Second Edition, John Wiley and Sons, New York.

Lucken, E.A.C., 1969, Nuclear Quadrupole Coupling Constants, Academic Press, London.

Mangum, B.W. and Utton, D.B., 1967, Bull. Am. Phys. Soc., 12, 1043.

Matcha, Robert L., 1970, J. Chem. Phys., 53, 485.

Morosin, B., 1968, J. Chem. Phys., 49, 3007.

Parks, S.I., 1967, dissertation, N.M.R. in Paramagnetic $NdBr_3$ and UI_3 and in Antiferromagnetic UI_3, Florida State University.

Ramsey, N.F., 1956, Molecular Beams, Oxford University Press, London, Table XI.

Raymond, Michael, 1971, Phys. Rev. B., 3, 3692.

Sawatzky, G.A. and Hupkes, Julieks, 1970, Phys. Rev. Letters, 25, 100.

Sharma, R.R. and Das, T.P., 1964, J. Chem. Phys., 41, 3581.

Sharma, R.R., 1970, Phys. Rev. Letters, 25, 1622.

Sharma, R.R., 1971, Phys. Rev. Letters, 26, 563.

Slichter, C.P., 1963, Principles of Magnetic Resonance, Harper & Row, New York.

Stedman, G.E. and Newman, D.J., 1971, J. Chem. Phys., 55, 152.

Sternheimer, R. and Foley, H., 1956, Phys. Rev., 102, 731.

Taylor, D.R., 1968, J. Chem. Phys. 48, 536.

Templeton, D.H. and Dauben, C.H., 1954, J. Am. Chem. Soc., 76, 5237.

Varsanyi, F. and Maita, J.P., 1965, Bull. Am. Phys. Soc., 10, 609.

Wolcott, Norman M., 1959, J. Chem. Phys., 31, 536.

Zachariasen, W.H., 1948, J. Chem. Phys., 16, 254.

APPENDICES

APPENDIX A

LATTICE CONSTANTS AND POSITIONAL PARAMETERS

Morosin (1968) measured the lattice constants of $LaCl_3$, $NdCl_3$, $EuCl_3$ and $GdCl_3$ with an uncertainty of less than 0.001 Å. He also measured the chloride positional parameters to within 0.1%. He suggests the following procedure, based on the earlier work of Templeton and Dauben (1954), for estimating the lattice constants and positional parameters of $CeCl_3$, $PrCl_3$ and $SmCl_3$. When plotted against atomic number, the value for C obeys a smooth relationship while the value for A obeys two linear relationships, one for $LaCl_3$ through $NdCl_3$, and a second for $SmCl_3$ through $GdCl_3$. These graphs are shown in Figure A.1.

Values of u for $CeCl_3$ and $PrCl_3$ were obtained by linear interpolation of Morosin's data between $LaCl_3$ and $NdCl_3$, while the value for $SmCl_3$ was obtained by extrapolating the values for $EuCl_3$ and $GdCl_3$. Morosin's values for v obey a smooth curve from $LaCl_3$ through $EuCl_3$. Values of v for $CeCl_3$, $PrCl_3$ and $SmCl_3$ were interpolated from this curve. The curves for u and v are shown in Figure A.2. The interpolated values together with Morosin's data are listed in Table 2.1.

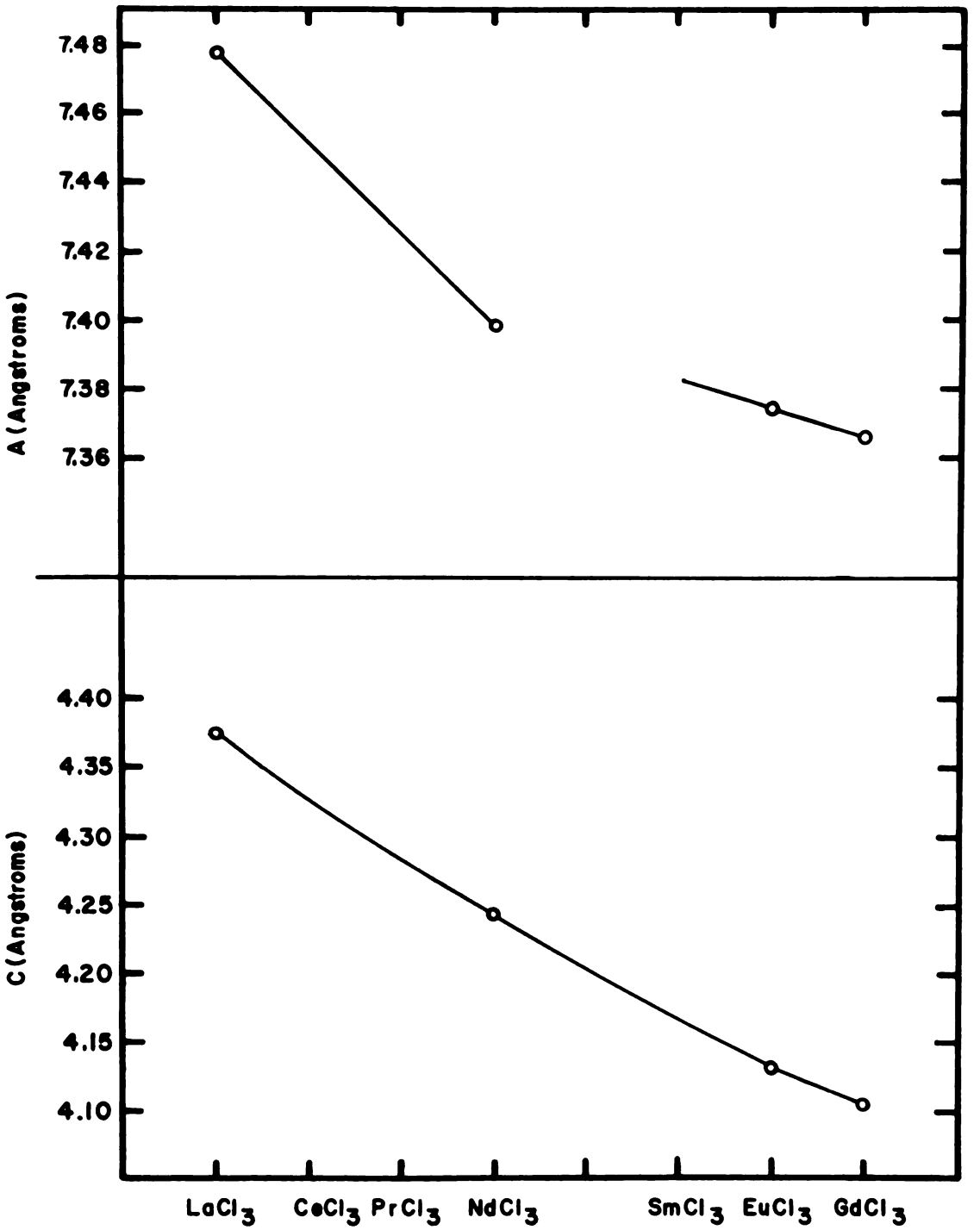

Figure A.1. Lattice Constants versus Compound

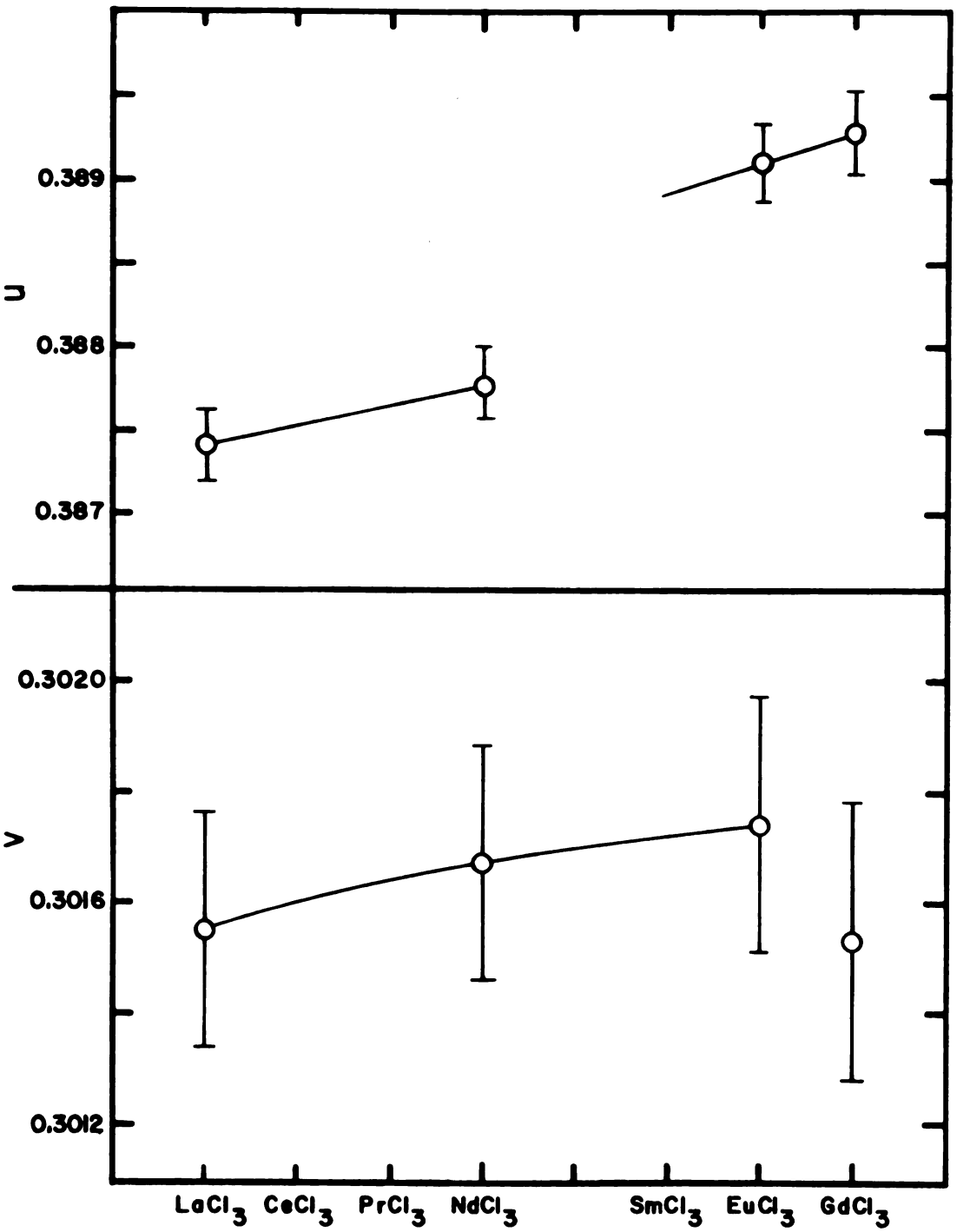

Figure A.2. Chloride Positional Parameters versus Compound

APPENDIX B

HEXAGONAL RARE EARTH TRICHLORIDE DATA

Raw data for the ^{35}Cl quadrupole resonance as a function of hydrostatic pressure at 77K and 300K is listed in Tables B.1 through B.5. Missing data at 300K indicates that signals were too weak to measure. In each table data is listed in the order in which it was recorded. All frequency values are the average of five readings with standard deviation of less than 1 kHz. The uncertainty in pressure values is judged to be 0.5×10^3 p.s.i. Data at 77K are plotted in Figures B.1 through B.5. On all graphs the size of the circle representing a datum is greater than the error associated with it. The room temperature data is similar to that at 77K. It is not plotted, but the results of a least squares analysis are presented in Table B.6.

Table B.1. Quadrupole Frequency versus Pressure Data: $CeCl_3$

Date	T = 77K	
	$P(10^3$ p.s.i.)	ν(kHz)
10/21/70	13.0	4356.9
10/21/70	19.6	4346.0
10/21/70	25.0	4335.7
10/21/70	30.0	4327.1
10/21/70	35.0	4317.9
10/21/70	39.9	4309.4
10/21/70	45.9	4299.6
10/21/70	50.2	4291.5
10/21/70	55.3	4282.7
10/21/70	61.2	4273.2
10/21/70	65.4	4266.2
10/21/70	70.3	4257.3
10/21/70	75.4	4248.9
10/21/70	81.2	4239.4
10/21/70	38.3	4312.8
10/21/70	52.7	4288.7
10/21/70	22.9	4339.6
10/21/70	8.1	4364.9
10/21/70	0.015	4377.2

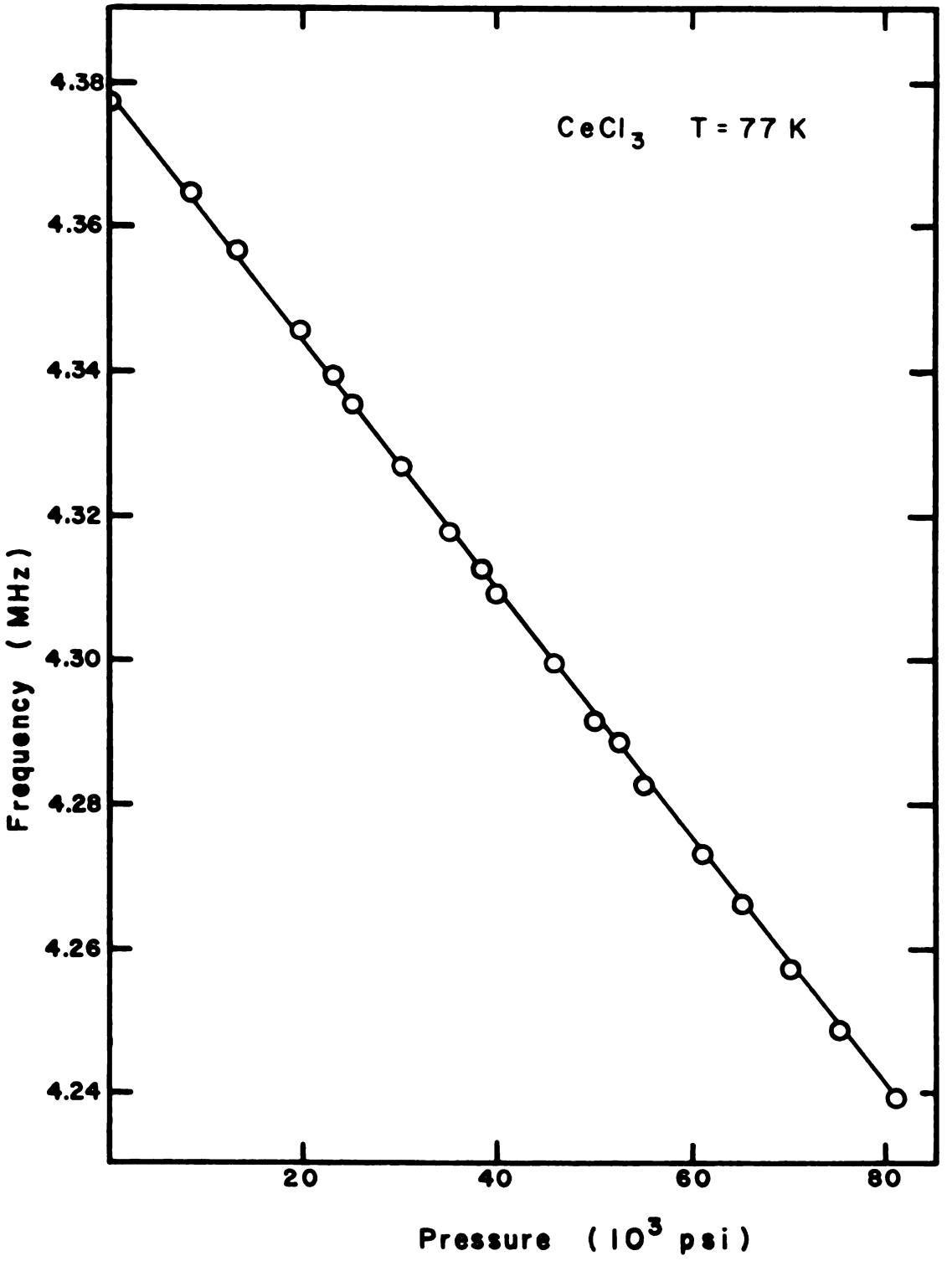

Figure B.1. Quadrupole Frequency versus Pressure at 77K: $CeCl_3$

Table B.2. Quadrupole Frequency versus Pressure Data: $PrCl_3$

Date	T = 77K	
	$P(10^3$ p.s.i.)	ν(kHz)
10/1/70	17.7	4533.3
10/1/70	40.7	4495.2
10/1/70	60.2	4462.3
10/8/70	23.1	4524.7
10/8/70	30.0	4513.5
10/8/70	39.9	4497.2
10/8/70	50.2	4479.0
10/8/70	60.0	4464.4
10/8/70	65.0	4455.9
10/8/70	70.7	4445.5
10/8/70	80.3	4430.4
10/8/70	75.7	4437.5
10/8/70	58.9	4464.9
10/8/70	0.015	4561.9

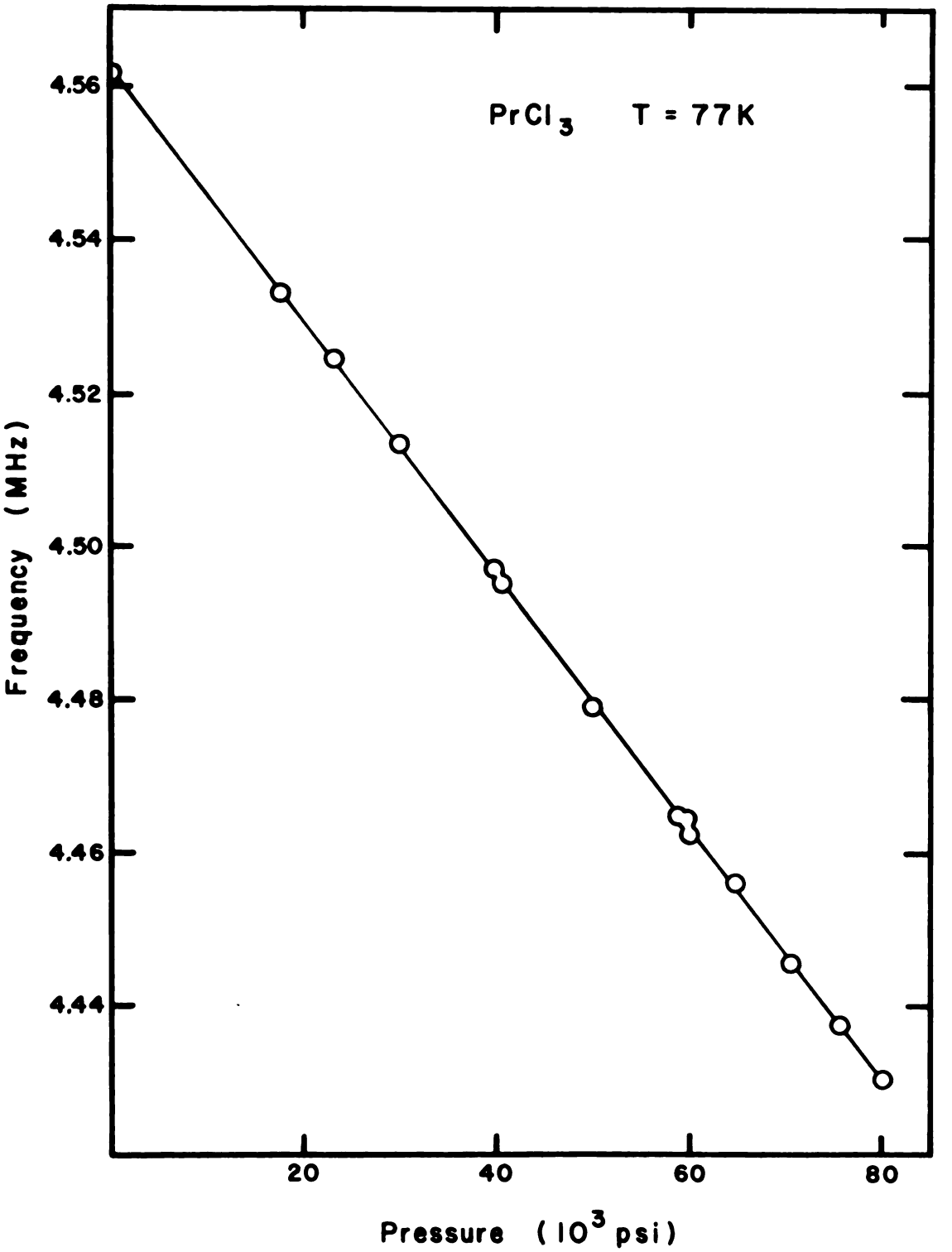

Figure B.2. Quadrupole Frequency versus Pressure at 77K: $PrCl_3$

Table B.3. Quadrupole Frequency versus Pressure Data: $NdCl_3$

Date	T = 77K	
	$P(10^3$ p.s.i.)	ν(kHz)
9/10/70	17.1	4696.1
9/10/70	40.9	4657.2
9/10/70	65.3	4620.0
9/10/70	53.0	4638.4
9/10/70	29.5	4675.8
9/10/70	17.1	4695.9
9/10/70	9.0	4708.6
9/10/70	5.0	4715.9
9/10/70	13.5	4702.0
9/10/70	19.9	4691.6
9/10/70	32.2	4671.3
9/10/70	43.8	4653.0
9/10/70	57.8	4631.1
9/10/70	62.0	4624.2
9/10/70	48.5	4646.0
9/10/70	37.2	4663.6
9/10/70	34.9	4667.7
9/10/70	24.9	4683.0
9/10/70	0.015	4722.3

Table B.3. (cont'd.)

Date	T = 300K	
	$P(10^3$ p.s.i.)	ν(kHz)
9/10/70	17.8	4649.6
9/10/70	40.9	4612.5
9/10/70	64.7	4574.8
9/10/70	51.5	4595.1
9/10/70	30.2	4628.9
9/10/70	17.8	4649.3
9/10/70	0.015	4676.4

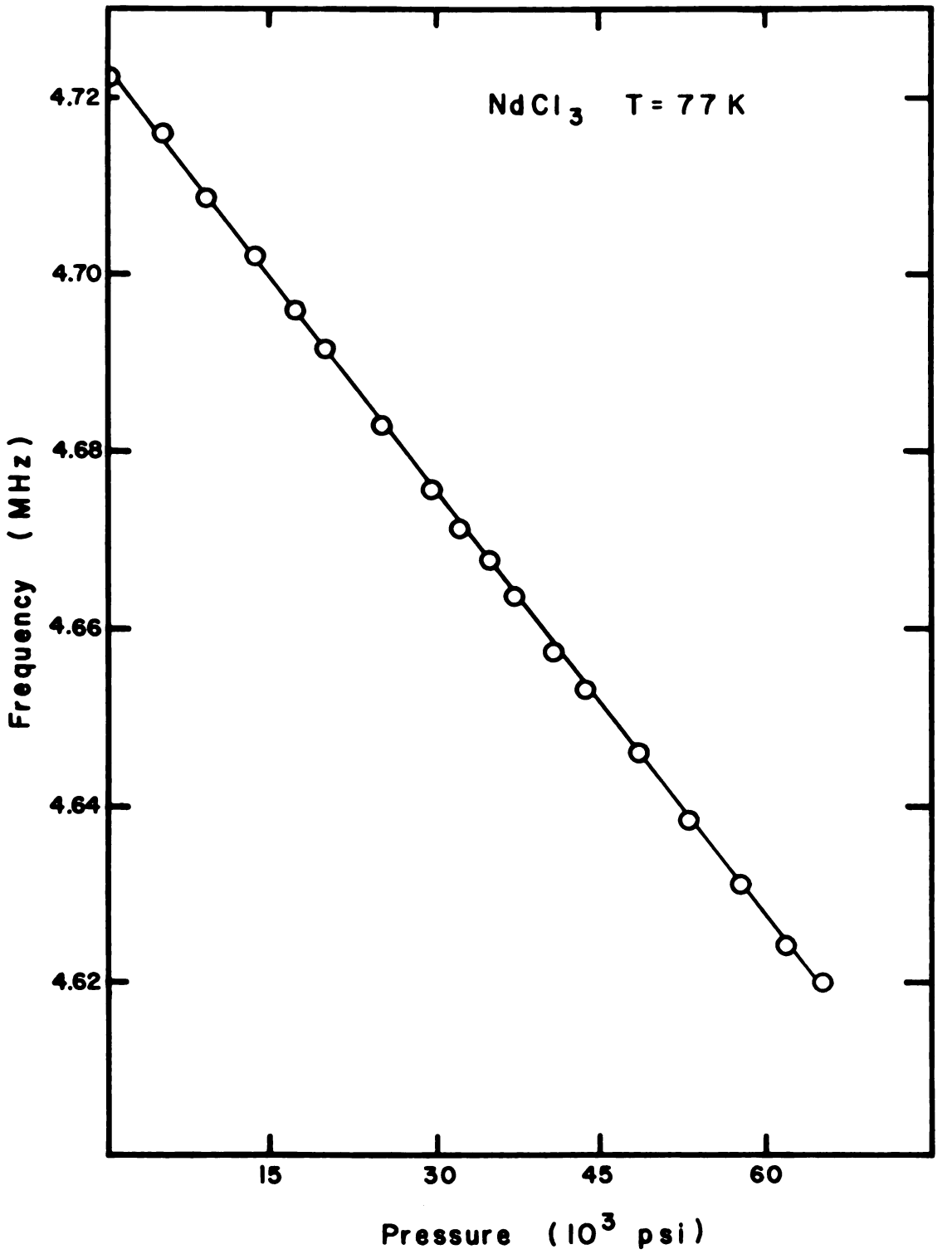

Figure B.3. Quadrupole Frequency versus Pressure at 77K: $NdCl_3$

Table B.4. Quadrupole Frequency versus Pressure Data: $SmCl_3$

Date	T = 77K	
	$P(10^3$ p.s.i.)	ν(kHz)
9/9/70	19.0	4999.4
9/9/70	40.9	4965.6
9/9/70	61.0	4937.2
9/9/70	67.0	4926.2
9/9/70	50.9	4950.1
9/9/70	30.9	4981.0
9/9/70	17.2	5001.6
9/9/70	25.0	4989.3
9/9/70	55.7	4943.0
9/9/70	45.2	4957.9
9/9/70	36.1	4972.3
9/9/70	8.6	5014.1
9/9/70	0.015	5026.8
	T = 300K	
	$P(10^3$ p.s.i.)	ν(kHz)
9/9/70	18.2	4950.7
9/9/70	41.0	4914.4
9/9/70	60.3	4887.2
9/9/70	0.015	4975.6

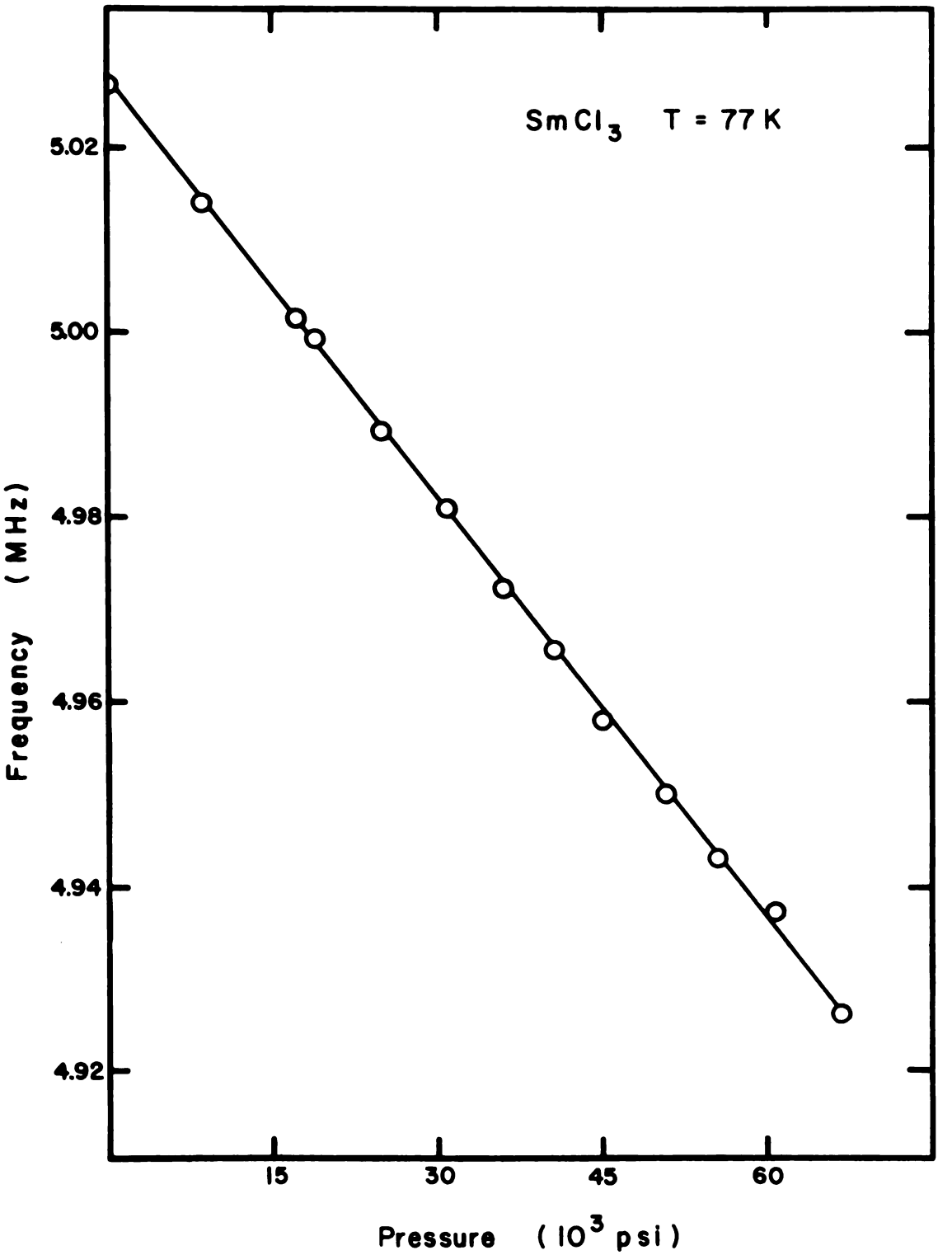

Figure B.4. Quadrupole Frequency versus Pressure at 77K: $SmCl_3$

Table B.5. Quadrupole Frequency versus Pressure Data: $GdCl_3$

Date	T = 77K	
	$P(10^3$ p.s.i.)	ν(kHz)
7/14/70	14.8	5286.9
7/14/70	22.2	5276.7
7/14/70	24.0	5274.4
7/15/70	10.5	5293.1
7/15/70	23.9	5274.0
7/15/70	45.3	5242.3
1/13/71	18.8	5281.9
1/13/71	30.0	5264.9
1/13/71	40.0	5251.5
1/13/71	49.8	5236.9
1/13/71	60.2	5221.4
1/13/71	69.2	5208.9
1/13/71	55.3	5229.6
1/13/71	45.7	5242.7
1/13/71	35.3	5257.4
1/13/71	25.0	5272.8
1/13/71	14.3	5288.5
1/13/71	7.8	5297.8
1/13/71	0.015	5307.6

Table B.5. (cont'd.)

Date	T = 300K	
	P(10^3 p.s.i.)	ν(kHz)
7/23/70	5.0	5241.5
7/23/70	10.0	5233.4
7/23/70	21.0	5220.4
7/23/70	30.0	5207.3
7/23/70	40.2	5190.7
7/23/70	50.2	5177.4
7/23/70	34.9	5199.5
7/23/70	25.1	5212.4
7/23/70	0.015	5248.4
1/13/71	59.6	5165.8
1/13/71	75.3	5144.1
1/13/71	45.7	5185.6
1/13/71	54.9	5174.0
1/13/71	64.9	5159.8
1/13/71	70.2	5152.0
1/13/71	19.6	5222.6

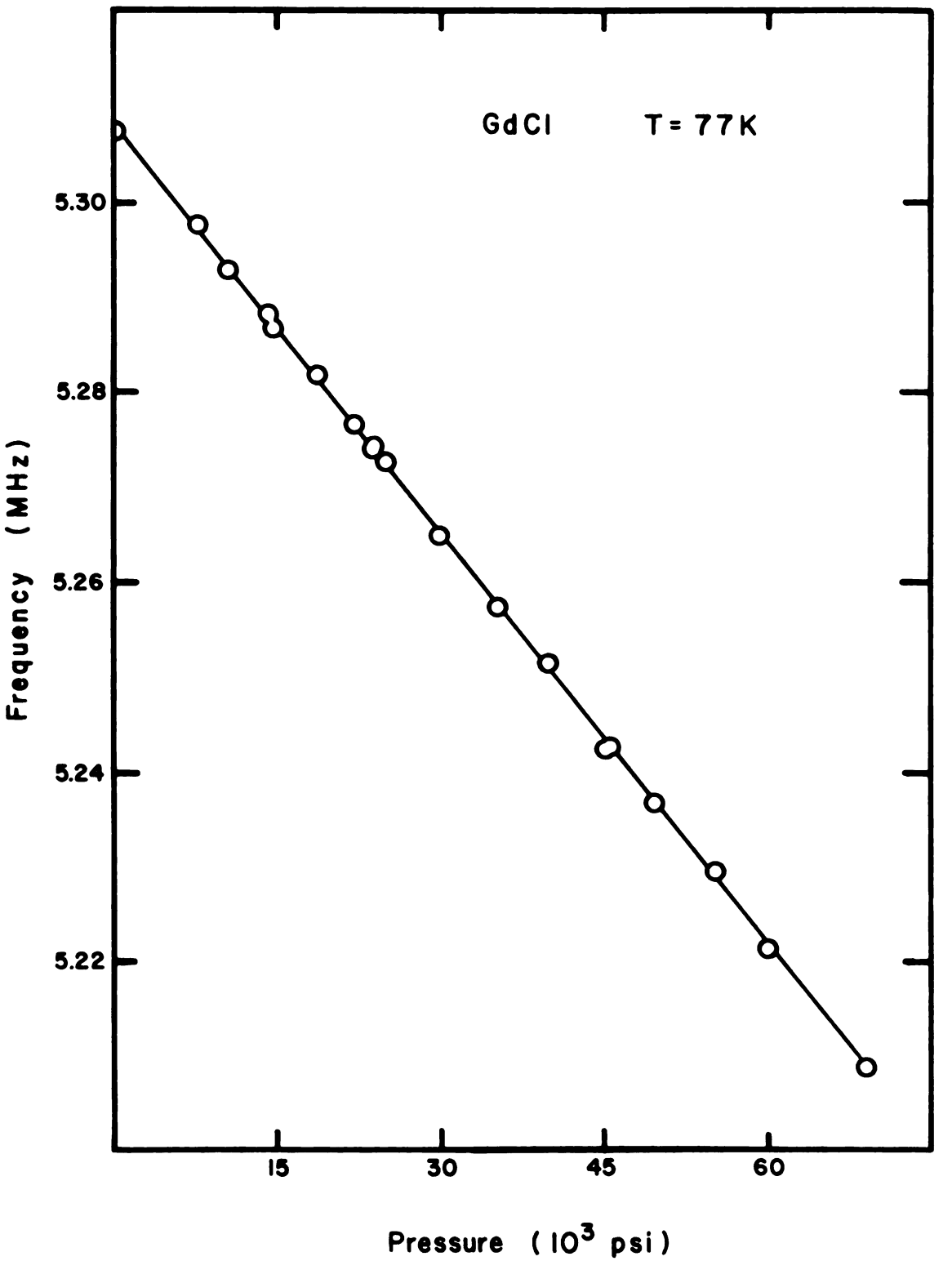

Figure B.5. Quadrupole Frequency versus Pressure at 77K: $GdCl_3$

Table B.6. Summary of Frequency versus Pressure Data at 300K

Compound	ν_Q(kHz)	ν_o(kHz)	$(\partial\nu/\partial P)_T$ (Hz/psi)	$\nu_o^{-1}(\partial\nu/\partial P)_T$ (10^{-6} cm^2/kg)
$NdCl_3$	4676.4 ± 0.3	4677.6 ± 0.4	-1.595 ± 0.010	-4.85 ± 0.03
$SmCl_3$	4975.6 ± 0.4	4976.3 ± 1.2	-1.482 ± 0.030	-4.24 ± 0.06
$GdCl_3$	5248.4 ± 0.3	5248.1 ± 0.5	-1.376 ± 0.012	-3.73 ± 0.03

APPENDIX C

DATA FOR $ErCl_3$ AND $YbCl_3$

$ErCl_3$ and $YbCl_3$ are isomorphic to monoclinic $AlCl_3$. There are two chemically inequivalent chloride ion sites in the molecule resulting in two quadrupole frequencies separated by about 50 kHz. The lower frequency line is twice as intense as the upper line. The former is referred to as ν_2 and the latter as ν_1.

The crystal structure parameters for these compounds are poorly known. For a summary of the locations of available data see Morosin (1968), reference 12. For this reason field gradient calculations in these compounds have not been carried out. During the course of this work, however, the pressure dependence of the quadrupole frequencies in $ErCl_3$ and $YbCl_3$ was measured.

In both compounds the quadrupole frequencies increase with pressure, each of the two lines in a given compound having a different slope. Raw data for the ^{35}Cl resonances is given in Tables C.1 and C.2. All data is for T = 77K, with the exception of the stronger line in $ErCl_3$ where some data at 300K was also taken. The data at 77K is plotted in Figures C.1 and C.2.

The resonance lines in $ErCl_3$ at 77K disappeared above a pressure of about 55×10^3 p.s.i., and did not reappear when the pressure was lowered. This effect was observed in two different samples, one of which was kept free of mineral oil. As the critical pressure was approached the

resonance signals lost strength. This probably means that the lines broadened. The effect was not observed at 300K at pressures up to 65 x 10^3 p.s.i. We suspect that what we observed was a crystallographic transition to the orthorhombic $TbCl_3$ structure. Monoclinic $DyCl_3$ is known to undergo such a transition when cooled to 77K (Carlson, 1969). No further investigation of the transition in $ErCl_3$ was attempted.

In $YbCl_3$ the lower frequency line has a distinct non-linear increase with pressure, while the upper line appears to be strictly linear. Since the data for $ErCl_3$ is of relatively poor quality such behavior there can not be ruled out. The results of a least squares analysis of the data for $ErCl_3$ and $YbCl_3$ are presented in Table C.3.

Table C.1. Quadrupole Frequency versus Pressure Data: $ErCl_3$

Date	T = 300K		
	$P(10^3$ p.s.i.)	ν_2(kHz)	ν_1(kHz)
9/8/70	19.7	4429.4	---[a]
9/8/70	50.5	4939.3	---
9/8/70	65.8	4444.8	---
9/8/70	46.3	4438.0	---
9/8/70	30.3	4433.2	---
9/8/70	0.015	4424.5	4476.8
	T = 77K		
	$P(10^3$ p.s.i.)	ν_2(kHz)	ν_1(kHz)
9/8/70	14.1	4454.9	4518.0
9/8/70	30.0	4460.3	4528.0
9/8/70	45.0	4466.5	4537.2
10/20/70	20.2	4456.5	4519.7
10/20/70	26.0	4458.8	4525.0
10/20/70	32.0	4461.2	4529.5
10/20/70	38.0	4464.5	4532.1
10/20/70	44.0	4466.5	4537.0
10/20/70	50.2	4468.2	4539.6
10/20/70	20.1	4455.5	4520.2
10/20/70	54.5	4472.0	too weak
8/9/70	0.015	4449.2	4508.5

[a]Line not measurable.

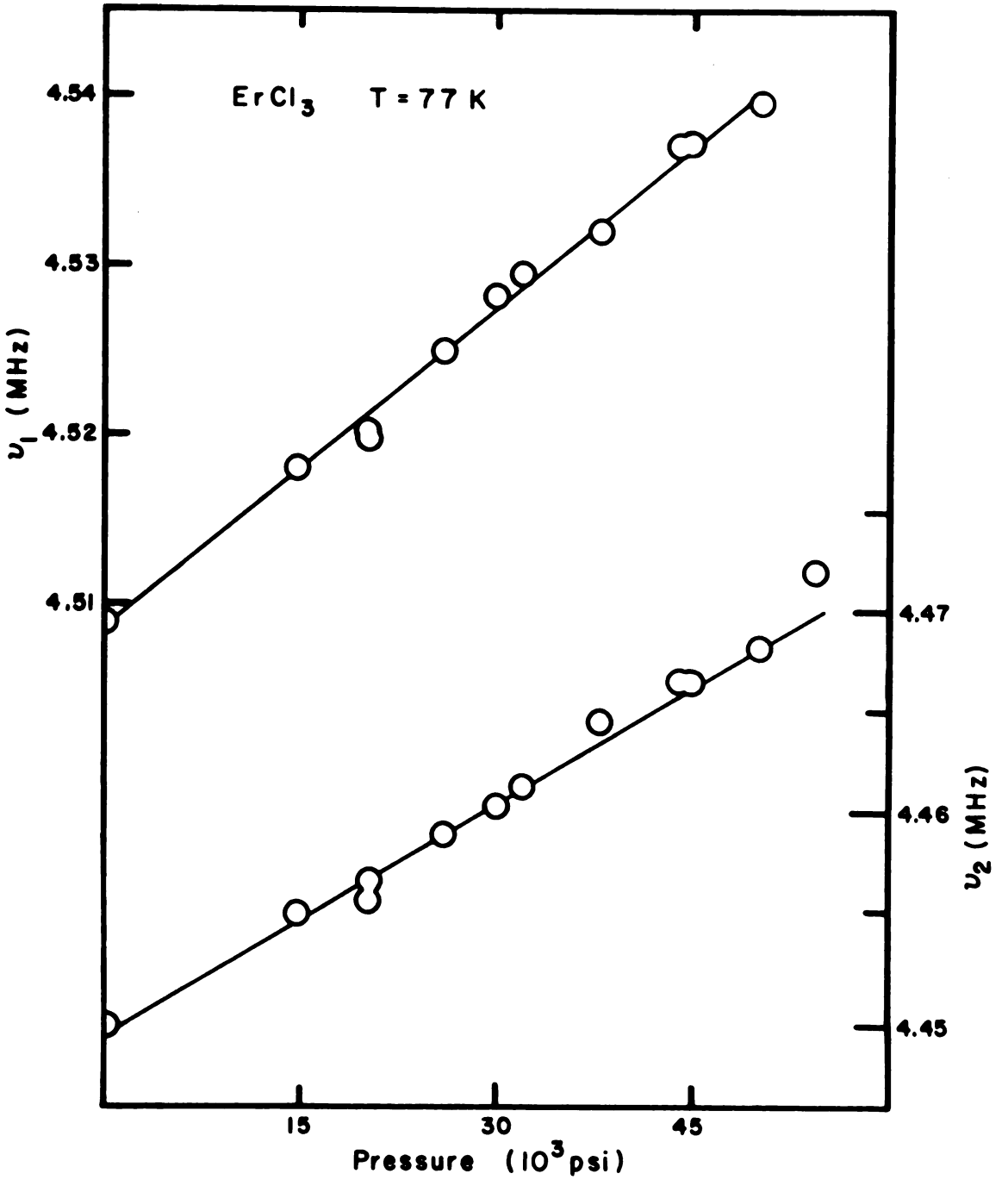

Figure C.1. Quadrupole Frequencies versus Pressure at 77K: $ErCl_3$

Table C.2. Quadrupole Frequency versus Pressure Data: $YbCl_3$

Date	T = 77K		
	$P(10^3$ p.s.i.)	ν_2(kHz)	ν_1(kHz)
1/15/71	21.8	4787.1	4847.8
1/15/71	24.9	4787.7	4849.6
1/15/71	30.0	4789.3	4852.6
1/15/71	35.0	4790.9	4854.9
1/15/71	40.1	4792.3	4857.4
1/15/71	45.0	4793.8	4860.6
1/15/71	50.4	4795.7	4863.3
1/15/71	55.0	4796.9	4865.9
1/15/71	60.2	4798.7	4868.9
1/15/71	65.2	4800.3	4871.3
1/15/71	70.0	4801.9	4874.1
1/15/71	75.3	4804.1	4877.3
1/15/71	80.5	4806.2	4879.0
8/9/70	0.015	4781.1	4836.0

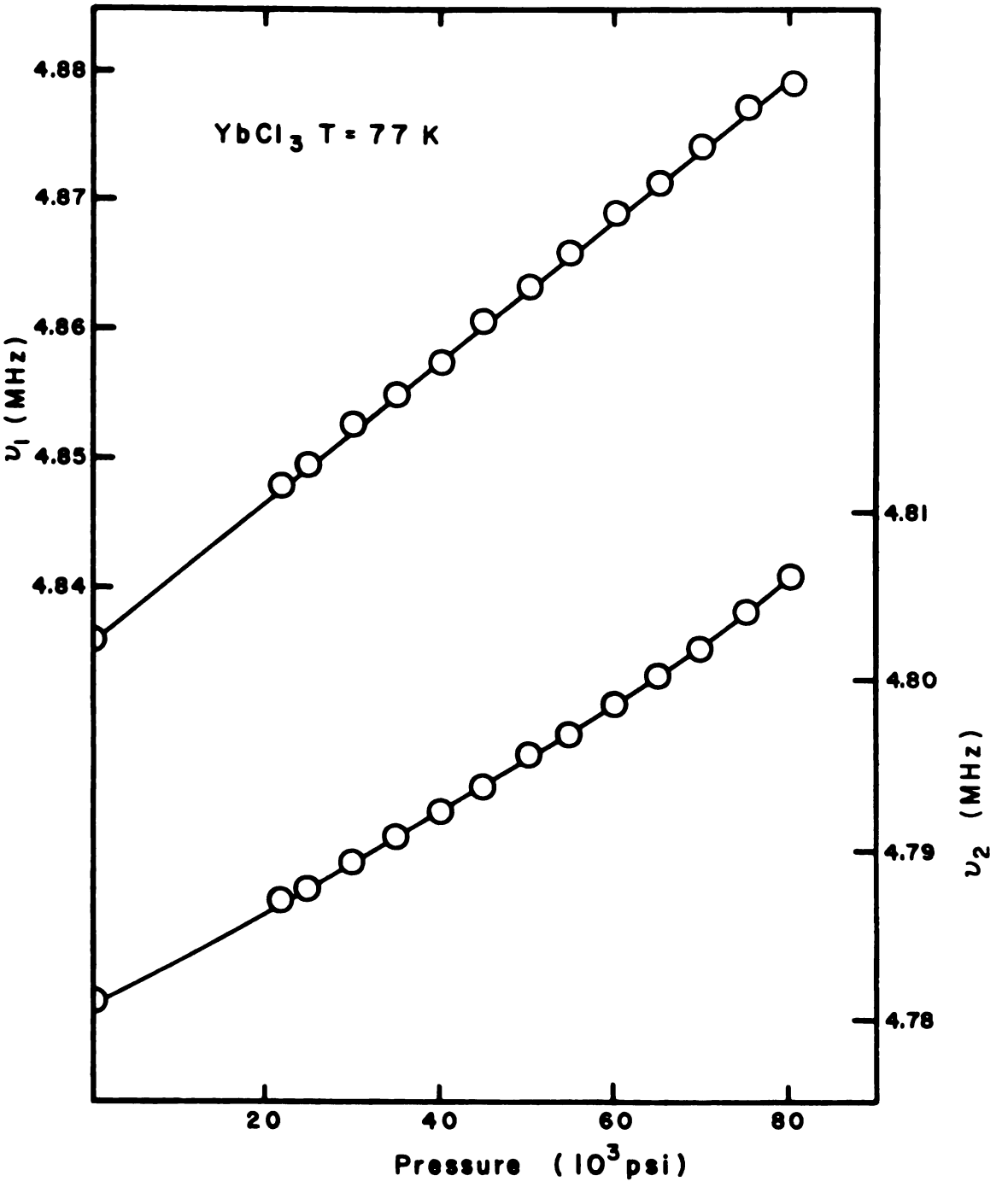

Figure C.2. Quadrupole Frequencies versus Pressure at 77K: $YbCl_3$

Table C.3. Pressure Coefficients at 77K for $ErCl_3$ and $YbCl_3$

T = 77K	ν_Q(kHz)	ν_o(kHz)	$(\partial\nu/\partial P)_T$ (Hz/psi)	$\nu_o^{-1}(\partial\nu/\partial P)_T$ (10^{-6} cm^2/kg)
$ErCl_3$[a]				
ν_2(kHz)	4449.2 ± 0.3	4447.8 ± 0.6	0.424 ± 0.016	1.36 ± 0.05
ν_1(kHz)	4508.5 ± 0.3	4507.8 ± 0.8	0.649 ± 0.023	2.05 ± 0.07
$YbCl_3$				
ν_2(kHz)	4781.1 ± 0.3	-----	0.26 ± 0.02[b]	0.77 ± 0.07[b]
ν_1(kHz)	4836.0 ± 0.4	4836.1 ± 0.2	0.541 ± 0.004	1.59 ± 0.01

[a]Signals in $ErCl_3$ vanished for pressures above 55 X 10^3 p.s.i.

[b]Curve is non-linear. Calculated for the zero pressure limit.

APPENDIX D

LATTICE SUMS

All lattice sums were computed from FORTRAN programs written for the CDC 6500 computer at Michigan State University. Sums were done over neutrally charged clusters of eight ions in a roughly spherical volume of radius 50 Å. Approximately 2500 such clusters were included in the sums. The components of the electric field gradient tensor were computed in a Cartesian frame defined by

$$x = \sqrt{3}\, a(A-B)/2 \ , \qquad \text{(D.1a)}$$

$$y = a(A+B)/2 \quad \text{and} \quad z = cC, \qquad \text{(D.1b)}$$

where a and c are the lattice constants, and A, B and C are distances along the (right-handed) crystallographic axes. The convergence of these sums was tested by comparing the results of a 50 Å sum with one of 100 Å. The results differed by less than 1 part in 10^4 for each component of the tensor.

In these calculations the contribution to the field gradient from an ion located at (x_1, x_2, x_3) is given by

$$V_{ij} = (Q_p - Q_o)(3x_i x_j - R^2\delta_{ij})/R^2, \ (i,j = 1,2,3). \qquad \text{(D.2)}$$

R is the distance to the ion with charge z and Q_p and Q_o are the point charge and overlap contribution given by

$$Q_p = z(1 - \gamma_\infty)/R^3 \qquad \text{(D.3)}$$

and

$$Q_o = F \exp[(R_{\alpha\beta} - R)/\rho_{\alpha\beta}] \quad . \qquad (D.4)$$

$R_{\alpha\beta}$ and $\rho_{\alpha\beta}$ are the soft-sphere parameters for the Cl^- ion at the origin and the particular ion at distance R. Q_o is included in the calcuation only for ions with $R \leq 4.0$ Å. F and $(1 - \gamma_\infty)$ are treated as adjustable parameters.

In the tables that follow the total electric field gradient is tabulated for the chloride ion at (u, v, 1/4). V_{xx}, V_{yy}, V_{zz} and V_{xy} are the components of the gradient in the Cartesian frame defined above. V_{xz} and V_{yz} are zero from symmetry. V_x, V_y and V_z are the diagonal elements of the field gradient tensor in its principal axis system. The relationship between the diagonal elements of the field gradient in atomic units ($bohr^{-3}$) and the quadrupole frequency is

$$\nu_Q = 9.3614\ V_z \sqrt{1 + \tfrac{1}{3}\eta^2}\ \text{MHz} \quad . \qquad (D.5)$$

Table D.1. Results of Point Charge Model

Compound	V_{xx}[a]	V_{yy}[a]	V_{zz}[a]	V_{xy}[a]	V_x[b]	V_y[b]	V_z[b]	η	ν(MHz)[c]
$LaCl_3$	0.40263	-0.47614	0.07351	0.01564	0.0735	0.4029	-0.4764	0.6914	4.802
$CeCl_3$	0.40963	-0.48451	0.07488	0.02488	0.0749	0.4103	-0.4852	0.6913	4.891
$PrCl_3$	0.41680	-0.49305	0.07625	0.03394	0.0762	0.4181	-0.4943	0.6915	4.983
$NdCl_3$	0.42358	-0.50119	0.07762	0.04288	0.0766	0.4255	-0.5031	0.6915	5.071
$SmCl_3$	0.43011	-0.51304	0.08293	0.06651	0.0829	0.4348	-0.5177	0.6796	5.206
$EuCl_3$	0.43149	-0.51907	0.08759	0.07714	0.0876	0.4377	-0.5253	0.6665	5.269
$GdCl_3$	0.43286	-0.52279	0.08992	0.08563	0.0899	0.4405	-0.5304	0.6609	5.314

[a] EFG components are in units of $bohr^{-3}$ and have been multiplied by $(1 - \gamma_\infty) = 17.59$.

[b] Diagonal elements of EFG in $bohr^{-3}$.

[c] $\nu = 9.3614$ MHz $bohr^{+3}$ $V_z \sqrt{1 + 1/3\,\eta^2}$.

Table D.2. Results of the Soft Sphere Model: Data Set A

Compound	V_{xx}^{a}	V_{yy}^{a}	V_{zz}^{a}	V_{xy}^{a}	V_{x}^{b}	V_{y}^{b}	V_{z}^{b}	η	ν(MHz)
$LaCl_3$	0.33398	-0.44253	0.10855	0.05352	0.1086	0.3377	-0.4462	0.5134	4.357
$CeCl_3$	0.34192	-0.45510	0.11319	0.06675	0.1132	0.3475	-0.4607	0.5086	4.4944
$PrCl_3$	0.34940	-0.46754	0.11814	0.08001	0.1181	0.3572	-0.4753	0.5029	4.633
$NdCl_3$	0.35611	-0.47932	0.12322	0.09246	0.1232	0.3662	-0.4894	0.4965	4.766
$SmCl_3$	0.36523	-0.50476	0.13954	0.12458	0.1395	0.3827	-0.5223	0.4656	5.063
$EuCl_3$	0.36641	-0.51718	0.15077	0.13809	0.1508	0.3875	-0.5383	0.4398	5.199
$GdCl_3$	o.36888	-0.52701	0.15812	0.14969	0.1581	0.3932	-0.5514	0.4264	5.316

[a]EFG components in $bohr^{-3}$.

[b]Diagonal elements of EFG in $bohr^{-3}$.

Table D.3. Results of the Soft Sphere Model: Data Set B

Compound	V_{xx}^{a}	V_{yy}^{a}	V_{zz}^{a}	V_{xy}^{a}	V_{x}^{b}	V_{y}^{b}	V_{z}^{b}	η	ν(MHz)
$LaCl_3$	0.32401	-0.43340	0.10939	0.05560	0.1094	0.3281	-0.4375	0.4999	4.262
$CeCl_3$	0.33311	-0.44655	0.11345	0.06916	0.1134	0.3392	-0.4526	0.4987	4.410
$PrCl_3$	0.34147	-0.45943	0.11796	0.08286	0.1180	0.3500	-0.4679	0.4958	4.556
$NdCl_3$	0.34882	-0.47161	0.12279	0.09586	0.1228	0.3599	-0.4827	0.4912	4.697
$SmCl_3$	0.36146	-0.50017	0.13871	0.12814	0.1387	0.3801	-0.5188	0.4653	5.029
$EuCl_3$	0.36382	-0.51417	0.15035	0.14149	0.1503	0.3861	-0.5364	0.4394	5.181
$GdCl_3$	0.36753	-0.52559	0.15806	0.15334	0.1581	0.3931	-0.5512	0.4265	5.314

[a]EFG components in $bohr^{-3}$.

[b]Diagonal elements of EFG in $bohr^{-3}$.

Table D.4. Results of the Soft Sphere Model: Data Set C

Compound	V_{xx}[a]	V_{yy}[a]	V_{zz}[a]	V_{xy}[a]	V_x[b]	V_y[b]	V_z[b]	η	ν(MHz)
$LaCl_3$	0.31654	-0.42669	0.11051	0.05709	0.1101	0.3209	-0.4310	0.4889	4.193
$CeCl_3$	0.32654	-0.44033	0.11379	0.07084	0.1138	0.3330	-0.4468	0.4907	4.347
$PrCl_3$	0.33560	-0.45357	0.11798	0.08484	0.1180	0.3446	-0.4626	0.4899	4.500
$NdCl_3$	0.34348	-0.46609	0.12261	0.09819	0.1226	0.3552	-0.4778	0.4868	4.646
$SmCl_3$	0.35880	-0.49702	0.13822	0.13055	0.1382	0.3783	-0.5165	0.4648	5.006
$EuCl_3$	0.36208	-0.51222	0.15014	0.14378	0.1501	0.3851	-0.5353	0.4390	5.169
$GdCl_3$	0.36674	-0.52486	0.15811	0.15581	0.1581	0.3932	-0.5513	0.4264	5.315

[a] EFG components in $bohr^{-3}$.

[b] Diagonal elements of EFG in $bohr^{-3}$.